The Astrophysical Journal, 978:88 (24pp), 2025 January 01 https://doi.org/10.3847/1538-4357/ad8d49

Sub-Alfvénic Turbulence: Magnetic-to-kinetic Energy Ratio, Modification of Weak Cascade, and Implications for Magnetic Field Strength Measurements

A. Lazarian[1], Ka Wai Ho[1,2], Ka Ho Yuen[2], and Ethan Vishniac[3]
[1] Department of Astronomy, University of Wisconsin-Madison, Madison, WI, 53706, USA; lazarian@astro.wisc.edu, kho33@wisc.edu
[2] Theoretical Division, Los Alamos National Laboratory, Los Alamos, NM 87545, USA; kyuen@lanl.gov
[3] Physics Department, Johns Hopkins University, Baltimore, MD 21218, USA; evishni1@jhu.edu
Received 2023 December 7; revised 2024 October 24; accepted 2024 October 24; published 2024 December 26

Abstract

We study the properties of sub-Alfvénic magnetohydrodynamic (MHD) turbulence, i.e., turbulence with Alfvén mach number $M_A = V_L/V_A < 1$, where V_L is the velocity at the injection scale and V_A is the Alfvén velocity. We demonstrate that MHD turbulence can have different properties, depending on whether it is driven by velocity or magnetic fluctuations. If the turbulence is driven by isotropic bulk forces acting upon the fluid, i.e., is velocity driven, in an incompressible conducting fluid we predict that the kinetic energy is M_A^{-2} times larger than the energy of magnetic fluctuations. This effect arises from the long parallel wavelength tail of the forcing, which excites modes with $k_\parallel/k_\perp < M_A$. We also predict that as the MHD turbulent cascade reaches the strong regime, the energy of slow modes exceeds the energy of Alfvén modes by a factor M_A^{-1}. These effects are absent if the turbulence is driven through magnetic fluctuations at the injection scale. We confirm our predictions with numerical simulations. Since the assumption of magnetic and kinetic energy equipartition is at the core of the Davis–Chandrasekhar–Fermi (DCF) approach to measuring magnetic field strength in sub-Alfvénic turbulence, we conclude that the DCF technique is not universally applicable. In particular, we suggest that the dynamical excitation of long azimuthal wavelength modes in the galactic disk may compromise the use of the DCF technique. We discuss alternative expressions that can be used to obtain magnetic field strength from observations and consider ways of distinguishing the cases of velocity and magnetically driven turbulence using observational data.

Unified Astronomy Thesaurus concepts: Magnetic fields (994); Interstellar magnetic fields (845); Astrophysical fluid dynamics (101); Magnetohydrodynamics (1964)

1. Introduction

Magnetized astrophysical fluids are turbulent due to the high Reynolds number of flows (P. A. Davidson 2004). The motions are described as plasma turbulence on small scales, i.e., ion inertia scale. At the same time, the magnetohydrodynamic (MHD) approach has been successfully applied to describe astrophysical phenomena in a variety of astrophysical settings. The magnetic field constrains the motions of charged particles perpendicular to the direction of the magnetic field. It decreases the viscosity perpendicular to the magnetic field of both fully and partially ionized gas (see Table 1. in G. L. Eyink et al. 2011). Observations testify that MHD turbulence is ubiquitous (see A. Lazarian et al. 2010; B. Burkhart et al. 2015) and affects key astrophysical processes, including phase transitions in the diffuse interstellar media (see K. H. Yuen et al. 2024), star formation (see C. F. McKee & E. C. Ostriker 2007), and cosmic ray propagation (see A. Lazarian et al. 2023).

In many astrophysical environments, MHD turbulence is sub-Alfvénic, i.e., Alfvén velocity exceeds the turbulent velocity, making magnetic effects dominant for the turbulent motions. This subject has been studied less than trans-Alfvénic turbulence. This motivates our present study of sub-Alfvénic turbulence.

Astrophysical turbulence takes place in compressible media. However, the relative importance of compressibility effects differs from case to case. Many vital properties of MHD turbulence can be understood disregarding compressibility, i.e., considering incompressible MHD. This is similar to hydrodynamics, where the Kolmogorov theory, i.e., theory of incompressible turbulence, successfully explains many basic phenomena. Note that the theory of compressible hydrodynamic turbulence remains a rather unsettled subject (see P. A. Davidson 2004). Thus, we focus on the properties of incompressible sub-Alfvénic turbulence for the present study.

Incompressible turbulence is at the core of the MHD turbulence theory (see A. Beresnyak & A. Lazarian 2019, for a monograph). The properties of the Alfvénic mode cascade are marginally affected by media compressibility (J. Cho & A. Lazarian 2002). In a compressible medium, the Alfvénic mode slaves MHD motions corresponding to the slow mode, imposing its scaling on the slow mode (P. Goldreich & S. Sridhar 1995, henceforth GS95; Y. Lithwick & P. Goldreich 2001; J. Cho & A. Lazarian 2002, 2003). This makes the scaling of slow mode independent of compressibility effects. Alfvénic turbulence also determines magnetic field wandering (A. Lazarian & E. T. Vishniac 1999, hereafter LV99), giving rise to superdiffusive dispersion of magnetic field lines (LV99; G. L. Eyink et al. 2011; G. Eyink et al. 2013). In particular, the magnetic field wandering determines the observed variations of the direction of the dust polarization employed for obtaining magnetic field strength using the technique proposed by L. Davis (1951) and S. Chandrasekhar & E. Fermi (1953). The corresponding technique is widely used to obtain magnetic field strength for sub-Alfvénic molecular clouds. Further on, we refer to the aforementioned approach as the Davis–Chandrasekhar–Fermi (DCF) technique.

In the DCF technique, the 2D magnetic field direction dispersion measured through dust polarimetry is combined with the velocity dispersion measured spectroscopically from the same molecular cloud. This technique obtains magnetic field strength assuming the turbulence is dominated by Alfvénic motions, isotropic, and has an equipartition between the magnetic and kinetic energies.

The equipartition of magnetic field fluctuations and velocity fluctuations has been challenged empirically based on the analysis of compressible sub-Alfvénic MHD turbulence simulations (C. Federrath et al. 2016; J. R. Beattie et al. 2022). These and further studies attributed the measured energy disparity and other nonclassical properties of MHD turbulence to the effects of compressibility. This resulted in a suggestion that the traditional DCF technique is valid for incompressible Goldreich–Sridhar turbulence, while the technique should be modified to deal with compressible MHD turbulence in molecular clouds (R. Skalidis & K. Tassis 2021; R. Skalidis et al. 2021). The theoretical arguments supporting this modified technique require turbulence to be compressible.[4]

In this paper, we do not consider fluid compressibility, and thus we do not discuss the theories that appeal to compressibility to either describe the aforementioned properties of turbulence or justify the "compressible" modification of the DCF technique. Instead, we consider incompressible MHD turbulence and explore how its properties are affected by velocity versus magnetic driving at the injection scale. We test our theoretical finding by analyzing numerical simulations of incompressible 3D MHD turbulence.

Our study identifies that the velocity driving of MHD turbulence can be an alternative reason for the violation of kinetic and magnetic turbulent energies equipartition. This effect was not reported earlier in incompressible MHD because in most of the corresponding theory-motivated numerical studies of incompressible MHD turbulence (see A. Beresnyak 2012, 2014) the turbulence is driven via Elsässer variables, where magnetic field fluctuations are driven at the injection scale.

A good correspondence of some of our results to those identified earlier as arising from the compressibility of MHD turbulence is suggestive that the fluid compressibility may not be the reason for the reported nonclassical behavior of MHD turbulence. Since astrophysical simulations of turbulence are made with compressible codes that employed velocity driving (C. Federrath et al. 2008, 2016; J. R. Beattie et al. 2020, 2022; C. Federrath et al. 2021), we conjecture that the reported effects can universally arise from how turbulence is driven.

The rest of this paper is structured as follows. In Section 2, we describe how the properties of sub-Alfvénic turbulence near the injection scale can be modified by velocity driving. We describe our numerical simulations in Section 3 and test our theoretical prediction with 3D MHD numerical simulations of incompressible turbulence in Section 4. In Sections 5 and 6, we compare our findings with the results of earlier numerical simulations. The implications of our results for obtaining magnetic field strength from observations are discussed in Section 7. We discuss our results in Section 8 and give a summary in Section 9.

[4] The effects of compressibility are complicated and were frequently appealed to when researchers faced unexpected phenomena. For instance, the numerical discovery of MHD turbulence fast decay was surprising and originally attributed to energy transfer from Alfvénic to compressible dissipative motions (see J. M. Stone et al. 1998). In reality, this was a fundamental property of strong MHD turbulence, which is also present in the incompressible limit (see J. Cho & A. Lazarian 2002).

2. Sub-Alfvénic MHD Turbulence

Kolmogorov theory is a theory of hydrodynamic incompressible turbulence, which has shown a lot of practical applicability despite its assumption of incompressibility. In this section, we discuss the strong cascade of incompressible Alfvénic turbulence case to show its analogy to the Kolmogorov theory. This will provide intuitive guidelines for addressing the case of weak cascade of Alfvénic turbulence that demonstrates more facets depending on its driving and boundary conditions.

2.1. Lessons from Strong Cascade of Alfvénic Turbulence

2.1.1. Local System of Reference for Turbulent Motions

The theory of MHD turbulence can be traced to the classical studies by P. S. Iroshnikov (1964) and R. H. Kraichnan (1965), which, however, missed its major property, i.e., its anisotropy (see J. C. Higdon 1984). In GS95, the theory of MHD turbulence describing its anisotropic nature was formulated for Alfvén Mach number

$$M_{A,b} \equiv \frac{V_{L,b}}{V_A} = \frac{\delta B_L}{B}, \quad (1)$$

equal 1, where $V_{L,b}$ is the injection velocity of Alfvénic or pseudo-Alfvénic (i.e., the slow modes in the incompressible regime) fluctuations at the injection scale L and V_A is the Alfvén velocity. Pseudo-Alfvénic fluctuations are the incompressible limit of slow MHD fluctuations, and they have fluctuations in velocity and magnetic field related through the Alfvén relation. Thus, the second relation in Equation (1) expressing $M_{A,b}$ follows automatically. In other words, GS95 is the theory of incompressible MHD turbulence in a trans-Alfvénic regime.

The original formulation's frequently overlooked limitation is that it did not include a fundamental notion of the local system of reference. The closure relations justifying the GS95 scaling were obtained in the generally accepted at that time reference frame related to the mean magnetic field. The problem is that, in reality, the fluctuations parallel and perpendicular to the mean magnetic field do not follow GS95 scaling, as was shown in subsequent numerical studies (see J. Cho & E. T. Vishniac 2000). Instead, magnetic fluctuations must be measured in the local system of reference defined by the direction of the magnetic field in the direct vicinity of the perturbation under study. The necessity of measuring turbulent fluctuations with respect to the direction of the magnetic field that directly affects these fluctuations became obvious in LV99, where the inseparable connection of Alfvénic turbulence and turbulent reconnection was demonstrated. In numerical studies by J. Cho & E. T. Vishniac (2000) and J. Maron & P. Goldreich (2001), it was demonstrated that it is only in the local system of reference that the GS95 relation between the parallel and perpendicular to magnetic field turbulent motions is satisfied. In what follows, we denote these scales $l_\parallel$ and $l_\perp$, keeping in mind that they are measured with respect to the local direction of the magnetic field.

2.1.2. Strong MHD Turbulence for $M_{A,b} < 1$

The incompressible MHD turbulence theory extension for the regime of $M_{A,b} < 1$ was performed in LV99. In the latter study, it was shown that Alfvénic turbulence with $M_{A,b} < 1$ exhibits at the injection scale the weak regime, which transfers to the strong GS95-like regime for smaller scales. The "weak" and "strong" are understood in terms of nonlinear interactions, i.e., the relation of the cascading time τ_{cas}, and the period of Alfvénic perturbation $t_A \sim \omega^{-1} \sim l_\parallel / V_A$. The weak turbulence corresponds to $\tau_{cas} > t_A$, and the strong turbulence corresponds to $\tau_{cas} \sim t_A$. The two regimes are not related to the amplitude of the fluctuations and turbulence with a relatively large amplitude of fluctuations can be found in the weak regime, while turbulence with a smaller amplitudes can be found in the strong regime. In what follows, we present an intuitive picture of the strong MHD turbulence cascade that follows from the LV99 theory of turbulent reconnection (see A. Lazarian et al. 2020 for a review).

Kolmogorov hydrodynamic turbulence (A. Kolmogorov 1941) can be described as eddies following Richardson's intuitive picture (see L. F. Richardson 1922). According to this picture, the large eddies generate smaller eddies until the viscosity damps the smallest eddies. Transferring energy from the driver to eddies is advantageous due to minimal resistance to the induced motions. On the contrary, inducing wave motions requires actions against the restoring force. Thus, given a choice, the kinetic energy is expected to transfer to eddies if eddy formation is possible.

In the presence of a magnetic field, it was traditionally assumed that the field prevented eddy motions. Thus, the case of MHD turbulence was traditionally considered in terms of interacting waves (P. S. Iroshnikov 1964; R. H. Kraichnan 1965). This, however, disregarded the possibility of exciting the eddy-like motions by mixing magnetized fluid perpendicular to the direction of the magnetic field. The existence of such eddies follows from the turbulent reconnection theory (LV99), as we discuss below.

For turbulent fluid, the direction of the magnetic field varies in space. Therefore, to define the direction of these mixing motions, one should consider the magnetic field in the eddy's vicinity, i.e., to define the local direction of the magnetic field. This revealed an analogy between the hydrodynamic and Alfvénic turbulence, making evident why, in GS95, the Kolmogorov spectrum of velocity fluctuations is expected.[5]

If one considers Alfvénic eddy-type motion of scale $l_\perp$ mixing magnetic field perpendicular to the direction of the local magnetic field, the kinetic energy of turbulent motions at the scale $l_\perp$ is $\sim \rho v_l^2$, where ρ is constant for incompressible turbulence. In terms of hydrodynamic equations, the nonlinear term for perpendicular motions that we consider is $(v\nabla)v \sim v_\perp^2/l_\perp$, which can be rewritten as $v_\perp \omega_{nl}$, where $\omega_{nl} \sim v_\perp / l_\perp$.

It is natural to associate τ_{cas} with the nonlinear time of the eddy turnover time $\tau_{turn} \sim l_\perp / v_l$. The latter condition is satisfied in the presence of turbulent reconnection (LV99) that predicts the reconnection time of the magnetic field in the eddy to be the eddy turnover time τ_{turn} for the eddies rotating perpendicular to the direction of the magnetic field. Thus, v_l should be identified with the eddy rotation perpendicular to the magnetic field. The hydrodynamic-like energy cascade involving such eddies corresponds to $v_l^2/\tau_{cas} \sim v_l^3/l = \text{const}$, providing the well-known Kolmogorov scaling of velocity fluctuations $v_l \sim l^{1/3}$.

Overall, the cascading of eddies aligned with the ambient magnetic field is similar to that of hydrodynamic eddies. Thus, the hydrodynamic-like character is relevant to perpendicular to magnetic field motions. The direction of the magnetic field surrounding the eddy, i.e., the local magnetic field, can be practically defined using structure functions (J. Cho & E. T. Vishniac 2000).

2.1.3. Scaling and Anisotropy for Strong MHD Turbulence for $M_{A,b} < 1$

The eddy motions of the magnetized fluid induce Alfvén waves with the period $\sim l_\parallel / V_A$, where $l_\parallel$ is the parallel scale of the eddy, which, as we mentioned earlier, should be measured in respect to the local direction of the magnetic field. Therefore, the critical balance condition postulated in GS95, should be written in the local system of reference as

$$l_\perp / V_l \approx l_\parallel / V_A. \quad (2)$$

Equation (2) reflects that the magnetic field eddy mixing perpendicular to the magnetic field induces the Alfvénic perturbation that defines the parallel to the magnetic field eddy scale. Recalling the definitions of the nonlinear and Alfvénic interactions, Equation (2) can be rewritten as $\omega_{nl} \approx t_A^{-1}$.

Naturally, the condition given by Equation (2) is not satisfied if the motions are considered in the mean magnetic field frame. Incidentally, in the eddy picture, the decay of strong Alfvénic turbulence in one Alfvén crossing time is expected because it is well known that hydrodynamic turbulence decays in one eddy turnover time.

To summarize, the strong Alfvénic turbulence, e.g., the turbulence corresponding to $M_{A,b} = 1$, as the case for the GS95 theory, can be presented as a collection of eddies aligned with the magnetic field surrounding the eddies. Thus, the eddies aligned with the surrounding magnetic field are involved in hydrodynamic-type motion. Naturally, the energy is channeled along this path of minimal resistance, and thus the energy of random driving mostly resides with the eddy cascade.

Consider a case of isotropic turbulence driving for strongly magnetized medium, i.e., for $M_{A,b} < 1$. It is obvious that if both injection parallel and perpendicular scales are equal to L, the critical balance condition given by Equation (2) cannot be satisfied. Thus, the GS95 theory of strong Alfvénic turbulence is not applicable at the injection scale. This is the domain of weak Alfvénic turbulence that we consider further in Section 2.2.

At the same time, there are no limitations to applying the critical balance to sufficiently small eddies. As the turbulent injection velocities decrease compared to Alfvén velocity V_A, the eddies get more elongated parallel to the local magnetic field direction. LV99 showed that in the latter case, the GS95 relations are modified to include Alfvén Mach number

[5] The discussion whether the turbulence has Iroshnikov–Kraichnan $\sim k^{-3/2}$ or Kolmogorov $\sim k^{-5/3}$ spectrum proceeded for several years (see A. Beresnyak & A. Lazarian 2006, 2009; S. Boldyrev 2006, 2007), but in our opinion the compelling evidence for the Kolmogorov spectrum is demonstrated in A. Beresnyak (2014). Note that the theories advocating the Iroshnikov–Kraichnan spectrum predict anisotropies that strongly disagree with numerical simulations (A. Beresnyak & A. Lazarian 2019).

dependence:

$$v_l \approx V_L\left(\frac{l_\perp}{L}\right)^{1/3} M_{A,b}^{1/3}, \quad (3)$$

and

$$l_\parallel \approx L\left(\frac{l_\perp}{L}\right)^{2/3} M_{A,b}^{-4/3}, \quad (4)$$

An essential property of the cascade is that according to Equation (3) the rate of nonlinear interactions increases with the decrease of the scale, i.e., $\omega_{nl} \sim l_\perp^{-2/3}$. This means this strength increases with the decrease of the scale of the turbulent motions, even though the amplitude of the fluctuations decreases.

We are interested in our present study in the $M_{A,b} < 1$ regime. First, it is important to define the applicability of the critical balance. It is evident from Equation (4) that for the perpendicular scale

$$l_{tr} = LM_{A,b}^2, \quad (5)$$

the parallel scale of magnetic eddies reaches the injection scale L. This value of $l_\perp$ defines the boundary of the applicability of the magnetic eddy-type turbulence, or the strong MHD turbulence. While the perpendicular cascade corresponds to the Kolmogorov one in terms of the energy spectrum, the parallel velocities v_l scale as $l_\parallel^{1/2}$, which corresponds to the parallel to magnetic field spectrum $\sim k_\parallel^{-2}$. When the spectra are averaged for a given $|k|$, the dominant contribution comes from the perpendicular fluctuations providing $E_{\rm strong}(|k|) \sim k^{-5/3}$.

At the scale $l_{{\rm tr},\perp}$ for $M_{A,b} < 1$, the velocity value is $V_L M_{A,b}$, i.e., smaller than the injection velocity by a factor $M_{A,b} < 1$. The fluctuations in the strong turbulence regime are Alfvénic with magnetic field and velocity connected by the Alfvénic relation, i.e., equipartition is naturally satisfied. Thus, the amplitude of fluctuation of the magnetic field at $l_{{\rm tr},\perp}$ is

$$\delta B_{\rm max,strong} \approx \frac{V_L}{\sqrt{4\pi\rho}} M_{A,b}. \quad (6)$$

The picture changes for scaling at scales larger than $l_{\rm tr}$. This is a regime of weak turbulence (see LV99; S. Galtier et al. 2000; S. Nazarenko 2011). The parallel scale of Alfvénic waves induced by driving at the injection scale exceeds L at these scales. As we discuss further, this requirement makes the weak turbulence less robust than the strong one.

GS95 demonstrated that pseudo-Alfvén modes are passive and are slaved by Alfvénic cascade. Thus, the relations between the parallel and perpendicular scales of pseudo-Alfvén fluctuations are given by Equation (2). This conclusion is also true for $M_{A,b} < 1$ case for $l_\perp < l_{\rm tr}$.

2.2. Weak Turbulence Driven by Velocities: The Violation of the Energy Equipartition

2.2.1. Stiff Magnetic Field Lines

Energy can be injected into MHD turbulence in different forms. Below, we focus on the effects of energy injection via velocity fluctuations.

As $M_{A,b}$ decreases, the kinetic motions gradually have more difficulty in bending stiff magnetic field lines at the injection scale. Consider an extreme case of velocity driving corresponding to $M_{A,b} \to 0$ limit assuming magnetic field lines are extremely stiff. In other words, the timescale for perturbing magnetic field lines, parametrized by $\tau = (k_\parallel v_A)^{-1}$, is very large. In this setting, the only possible motions of magnetized conducting fluid correspond to the mixing of absolutely straight magnetic field lines, i.e., the motions with the parallel wavenumber $k_\parallel = 0$. Such perpendicular motions do not induce Alfvén waves or any other finite-time magnetic field fluctuations. No magnetic field bending corresponds to no energy of Alfvén waves. Within our thought experiment, in the limit of $k_\parallel = 0$, turbulent magnetic energy vanishes, in contrast with the case of strong turbulence for which magnetic E_B and kinetic E_K energies are in equipartition. In what follows, we consider finite $M_{A,b} < 1$. The magnetic field lines, in this case, are not rigid and magnetic turbulent energy is not zero. Nevertheless, through continuity, our thought experiment suggests that the equipartition sub-Alfvénic turbulence is not guaranteed, and for some types of driving, $E_K > E_B$ is expected.

To elucidate the basic properties of sub-Alfvénic MHD turbulence, our study deals with the incompressible case. Nevertheless, magnetic field compressions are possible in this case. In the thought experiment of an extremely rigid magnetic field above, one can consider nearly straight magnetic field lines being compressed in the perpendicular direction. These bunches of magnetic field lines present the $k_\parallel = 0$ incarnation of pseudo-Alfvén/slow modes. Unlike its Alfvénic counterpart for $M_A \to 0$, these motions are associated with turbulent magnetic energy. Thus, one can expect that the magnetic energy of the slow modes can exceed the energy of the Alfvénic modes for sub-Alfvénic turbulence.

Another effect not considered in the theory of strong turbulence is the fluid motion along the magnetic field lines. In the limit of $M_{A,b} \to 0$ and a random isotropic velocity driving at the injection scale L, this driving excites only parallel kinetic motions without any magnetic field perturbations. This effect persists for $M_{A,b} < 1$ because the random isotropic driving tends to move fluid in the direction of the least resistance, the direction along the magnetic field lines. (This effect disappears for $M_{A,b} > 1$ as the magnetic field gets pliable to bending.) Thus, random velocity driving for small $M_{A,b}$ can induce $E_K \gg E_B$ in terms of both parallel and perpendicular to magnetic field fluctuations. This effect is unrelated to fluid compressibility, so in this study we do not discuss the theories that attribute the numerically detected disparity of kinetic and magnetic energies to fluid compressibility (see J. R. Beattie et al. 2022; R. Skalidis et al. 2023a).

One can consider magnetic field lines as parallel, nearly rigid tubes to understand driving low $M_{A,b}$ turbulence. Such intuitive treatment is congruent with several recent in situ solar wind studies (S. Banerjee & S. Galtier 2013; L. P. Yang et al. 2019; S. Zhao et al. 2024a, 2024b). The perpendicular motion of these tubes marginally deforms them. At the same time, the fluid can be pumped along the tubes without deforming them much. Both types of motion involve kinetic motions, while inducing a marginal energy transfer into the elastic stress energy. The latter is the analog of the magnetic perturbation energy.

The fluid flow along the magnetic field lines causes variations in the magnetic field tension. For a flow with velocity $V_{L,\parallel}$ along magnetic field lines, the Bernoulli equation

(see G. K. Batchelor 2000), in the absence of gravity, provides $P + \rho V^2/2 = \text{const}$, where P is the pressure of the fluid. If the velocity of fluid moving along the magnetic tube embedded in the media with external pressure P_0 changes in point 1 from V_1 to V_2 at point 2, the change of the fluid pressure changes from P_1 to P_2 according to the equation

$$P_0 + P_1 + 1/2\rho V_1^2 = P_0 + P_2 + 1/2\rho V_2, \tag{7}$$

resulting in

$$B\delta B \approx 1/2\rho(V_2^2 - V_1^2), \tag{8}$$

where we accounted that the changes in the fluid pressure induce the changes in the magnetic pressure according to $P_1 - P_2 = \delta P \approx B\delta B$. The fluctuation δB can be positive or negative depending on whether the amplitude of V_1 or V_2 is larger. Taking squares of both parts of Equation (8), one can determine the variance of the magnetic field fluctuations $(\delta B)^2$ and the standard deviation, which is the square root of the variance, i.e., $|\delta B|$.

For turbulent driving, it is natural to associate the maximal velocity difference with the velocity at the driving scale, i.e., $V_{L,\parallel}^2 \approx \max\{V_2^2 - V_1^2\}$. Therefore, one can write the resulting equation as

$$\rho V_{L,\parallel}^2 \approx B|\delta B_\parallel|. \tag{9}$$

The regions corresponding to higher fluid pressure result in the bulging of magnetic field lines, locally decreasing $\delta B_\parallel$, and the regions of lower fluid pressure result in getting magnetic field lines closer together, inducing magnetic field backreaction.

Later, in Section 5.2, we discuss that while Equation (9) resembles Equation (32), which was used in R. Skalidis & K. Tassis (2021, hereafter ST21), their physical reasoning and justification are very different from ours. In our approach, Equation (9) describes the response of the magnetic field to the change of the pressure in the flow of fluid that is independent of turbulence compressibility. At the same time, in ST21, Equation (32) is employed to describe the balance of kinetic and magnetic energies in a compressible MHD turbulence. In Section 5.2, we acknowledge our confusion with the theoretical arguments justifying the latter approach. At the same time, our derivation of Equation (9) also holds in the compressible case, which may reflect the universal property of sub-Alfvénic turbulence driven by isotropic velocity fluctuations.

The fluctuations of the magnetic field parallel to the mean magnetic field $\delta B_\parallel$ induce the magnetic field fluctuations perpendicular to the mean-field direction $\delta B_\perp$. This is a consequence of the divergence-free magnetic field, i.e., $\nabla\delta\boldsymbol{B} = \boldsymbol{0}$. Taking the z-axis along the mean magnetic field $\boldsymbol{B}$, one can write the divergence in the Cartesian coordinate system:

$$\frac{\partial\delta B_x}{\partial x} + \frac{\partial\delta B_y}{\partial y} + \frac{\partial\delta B_z}{\partial z} = 0, \tag{10}$$

where $\delta B_\perp = \sqrt{\delta B_x^2 + \delta B_y^2}$. At the injection scale, one can write $\partial\delta B_i \approx \delta B_i$, and $\partial x_i \approx L$, where $i = x, y, z$, where L is the scale of isotropic turbulence driving. This results in $-\delta B_x = \delta B_y + \delta B_z$ at the injection scale. Substituting this in the expression of perpendicular fluctuation, one gets for the energy of perpendicular fluctuations $\delta B_\perp^2 = 2\delta B_y^2 + 2\delta B_z\delta B_y + \delta B_z^2$. This change in the energy is a magnetic field response to a perturbation $\delta B_\parallel$. Naturally, the magnetic field resists perturbations and minimizes the increase of the energy induced by $\delta B_\parallel$.[6] For a given δB_z, the minimum of this energy corresponds to $\delta B_y \approx -\delta B_z/2$. The corresponding value of $\delta B_x \approx -\delta B_z/2$, which results in

$$\delta B_\perp \approx \delta B_\parallel. \tag{11}$$

In this paper, we do not consider the differences induced by solenoidal versus compressible driving of turbulence (see R. Skalidis et al. 2021). For incompressible fluids that we deal with, the latter driving is impossible. Our considerations that justify Equation (11) can also apply to the compressible case if the flow induces $\delta B_\parallel$. Note that numerical simulations in R. Skalidis et al. (2021) support Equation (11) for compressible MHD simulations. However, a more detailed discussion of the effects present in compressible sub-Alfvénic turbulence is beyond the scope of this paper.

By dividing both parts of Equation (9) by B and utilizing the definition of Alfvén velocity $V_A = B/\sqrt{4\pi\rho}$, one gets

$$\delta B \approx \sqrt{\rho} V_L\left(\frac{V_L}{V_A}\right), \tag{12}$$

where we used $\delta B = \sqrt{B_\parallel^2 + B_\perp^2}$ accounted for Equation (11). Equation (12) shows that for velocity driving, the fluctuations of magnetic field and velocity at the injection scale are not related through the Alfvén relations, but kinetic energy dominates for sub-Alfvénic velocity driving. This has significant implications, which we discuss further on in this paper.

A peculiar feature of our discussion above is that we did not separate the magnetic perturbations in fundamental MHD modes, i.e., slow, Alfvén, and fast. Instead, we deal with parallel and perpendicular magnetic field fluctuations $\delta B_\parallel$ and $\delta B_\perp$, which, as we discuss in the Appendix, can have a different way of decomposition into fundamental modes in media with different sound v_s and Alfvén velocity V_A ratios. Therefore, our estimates may apply to compressible simulations as discussed in Section 6.3. The sound velocity is much larger than the Alfvén velocity in the weakly compressible fluid, $v_s \gg V_A$. In this case, the fluctuations of velocity moving along the magnetic flux tube induce variations in the diameter that can be associated with slow modes. The same Bernoulli effect in the flux tube for $V_A \gg v_c$ induces the variations of flux tubes described by fast modes. In the Appendix, we explain in more detail how $\delta B_\parallel$ is produced by slow and fast modes in a more general setting. Both effects are described by Equation (9), i.e., the magnetic response of the media to sub-Alfvénic velocity driving does not depend on fluid compressibility. However, the case of incompressible MHD turbulence is simpler and more

[6] Formally, the divergence-free condition can also be satisfied if $\delta B_\perp$ is much larger than $\delta B_\parallel$. However, in the setting when hydrodynamic flows induce $\delta B_\parallel$ while $\delta B_\perp$ is induced to ensure the magnetic field is divergence free, the solutions with $\delta B_\perp$ larger than $\delta B_\parallel$ are not physical.

fundamental. Thus, for the rest of this paper, we will focus on it.

In the incompressible case, the extent of the magnetic field perpendicular dilatations, i.e., $LM_{A,b}$, determines the perpendicular coherence scale of the slow mode wavepackets. Further on in this paper, we discuss the consequences of this effect.

2.2.2. Relation to Strong Turbulence

For our discussion, it is important to keep in mind that nonlinearity is a property of fluids, not magnetic fields. The lessons that one can extract from our discussion of strong turbulence above are as follows:

1. In MHD, turbulence at small scales evolves through nonlinearities of the hydrodynamic equation term $(v\nabla)v \sim v_\perp^2/l_\perp$, where it is taken into account that the magnetic field constrains the parallel fluid motions. This results in the nonlinear rate of evolution $\omega_{nl} \sim v_\perp/l_\perp$. The nonlinearity comes from hydrodynamics with magnetic fields acting to restrict the possible fluid motions.
2. The nonlinear hydrodynamic term decorrelates motions within eddies, inducing the cascade of energy toward smaller scales.[7]
3. The critical balance given by $\omega_{nl} \sim t_A^{-1}$ (see Equation (2)) is the essential part of a strong turbulence regime. This induces the limit for the perpendicular scale of motions for strong turbulence given by Equation (5).

Extending this reasoning to the scales $[l_{tr,\perp}, L]$, we have to abandon point (3) above because the cascading rate ω_{nl} is smaller than the propagation rate t_A^{-1}. This is the point for which the physical picture that we considered earlier must be modified.

We may approach the problem of weak Alfvénic turbulence more formally, considering the three-wave interaction of waves with frequencies ω and wavenumber $\boldsymbol{k}$. The conservation of energy defined as $\omega_1 + \omega_2 = \omega_3$ should be satisfied together with the conservation of the momentum defined as $\boldsymbol{k}_1 + \boldsymbol{k}_2 = \boldsymbol{k}_3$ (see C. S. Ng & A. Bhattacharjee 1996). Accounting for the dispersion relation $\omega = \pm k_\parallel V_A$, one has to accept that in the weak regime there is no change of $k_\parallel$, but only the change of $k_\perp$ can occur. This means that the frequency of the waves in weak turbulence $\omega \sim k_\parallel V_A \sim V_A/l_\parallel$ does not change and stays equal to the frequency of waves at the injection scale L. This means that the cascading, i.e., the decorrelation of motions and higher spatial harmonics, appears only perpendicular to the magnetic field. This cascading happens over several t_A.

Like strong turbulence, weak turbulence is induced by motions perpendicular to the magnetic field. The weak turbulence cascade creates the pattern of filaments rotating perpendicular to the magnetic field. As these filaments get thinner than $l_{tr,\perp}$, the perpendicular fluid motions induce Alfvénic perturbations with frequency $\sim v_l/l_\perp$, invalidating the weak turbulence requirement of constant ω. This starts the regime of strong turbulence that we earlier described with the eddies. In other words, strong turbulence is a natural continuation of the weak cascade for the scales at which the magnetic field tubes get insufficiently rigid.

[7] This can be seen as a process of higher Fourier harmonics generation by the nonlinear term.

2.2.3. Velocity Scaling

Perpendicular velocity scaling. The nonlinear hydrodynamic term $\sim v_\perp/l_\perp$ induces cascading for the fluid moving along perturbed magnetic field lines. As we discussed earlier, the turbulent motions of weak Alfvénic turbulence are exclusively the motions perpendicular to the magnetic field, while ω does not change. The nonlinear hydrodynamic term distorts the original velocity pattern and creates more structure perpendicular to the magnetic field direction. The acceleration caused by this term is $v_\perp\omega_{nl}$ and it acts over the period of motion driving ω^{-1}. This induces a change of the momentum of the fluid element for incompressible fluid that is proportional to $v_\perp\omega_{nl}/\omega \sim v_k\chi$, where

$$\chi = \frac{(v_\perp/l_\perp)}{\omega}. \tag{13}$$

The restrictive role of the magnetic field is clear from Equation (13). The stronger the magnetic field, the larger ω and the smaller the nonlinear momentum change.

For weak turbulence, $\chi \ll 1$, meaning that magnetic field strongly inhibits nonlinearities. Thus, many nonlinear interactions are required to significantly decorate/cascade the velocity motions to smaller scales. In turbulence, the interactions are incoherent, which induces the random walk of the nonlinear distortion:

$$\delta v^2 \approx v_\perp^2\chi^2 N, \tag{14}$$

where $N \approx t\omega$ is the number of steps performed in time t. When the change of squared momentum δv^2 gets of the order of the original $\sim v_\perp^2$, the motions are randomized. This requires $N \sim \chi^{-2}$ steps.

This condition can be used to define the cascading time τ_{cas} of weak turbulence, i.e.,

$$\tau_{cas,weak}^{-1} \approx \frac{\omega}{N} \approx \frac{(v_l/l_\perp)^2}{\omega}, \tag{15}$$

where for the uniformity of the presentation with the case of strong turbulence, we used $l_\perp \sim k_\perp^{-1}$. Note that the cascading time given by Equation (15) is well accepted in the MHD turbulence literature (see R. H. Kraichnan 1965). We note that even though Equation (14) does not formally apply to strong turbulence, Equation (15) smoothly transfers to provide the correct cascading rate.[8]

The velocity scaling in weak turbulence can be derived trivially by noting that for weak turbulence $\tau_{cas,weak}^{-1} \ll \omega$ due to Equation (15). Since $l_\parallel$ does not change in the weak regime, ω stays constant. Therefore, the cascade of kinetic energy for $l_\perp$ in the range $[l_{tr,\perp}, L]$ can be described for incompressible motions as

$$v_{l,weak}^2/\tau_{cas,weak} \sim \frac{v_l^4}{l_\perp^2\omega} \sim \text{const}, \tag{16}$$

[8] For strong turbulence $\omega \sim V_A/l_\parallel$ changes with the scale $l_\parallel$ and provides $\tau_{cas,strong} \sim v_l/l_\perp$ due to Equation (15). This coincides with the hydrodynamic rate of eddy turnover around the direction of the magnetic field. The possibility of describing the strong turbulence as both eddies and waves corresponds to the duality of MHD turbulence nature discussed in J. Cho & A. Lazarian (2003).

which provides for weak MHD turbulence, i.e., for constant ω, the velocity scaling (LV99):

$$v_{l,\mathrm{weak}} \approx V_L \left(\frac{l_\perp}{L}\right)^{1/2}. \quad (17)$$

This scaling of velocity induces the scaling of kinetic energy $E_k \cdot k_\perp \sim v_k^2$, which results in

$$E_k \sim k_\perp^{-2}, \quad (18)$$

which is an accepted expression for the kinetic energy spectrum for weak turbulence (see LV99; S. Galtier et al. 2000).

Consider a toy model with an isotropic driving force δF. The increase of kinetic energy in a parallel direction is $\delta F \delta l$, with δ being the transposition of fluid over the time δt, i.e., $\delta l \sim a(\delta t)^2$, where the acceleration in parallel to magnetic field direction a is $\sim \delta F/\rho$. The injection velocity is $V_l \sim a\delta t$ in that direction. The transposition in the perpendicular to magnetic field direction is $M_{\mathrm{A},b}$ times smaller due to the backreaction of the magnetic tension. As a result, the energy induced by the isotropic driving in a perpendicular direction is reduced by a factor $M_{\mathrm{A},b}$ compared to the parallel direction. In other words, the amplitude of the kinetic energy associated with parallel to magnetic field motions $\mathcal{E}_\parallel$ is expected to be $\sim M_{\mathrm{A},b}^{-1}$ times the kinetic energy associated with perpendicular to magnetic field motions $\mathcal{E}_\perp$.

This agrees with the conclusion about the subdominance of the energy of magnetic turbulence fluctuations that follows from Equation (12). The cascade starts at the injection scale L for the isotropic driving.

Fluctuations in the flow parallel to the magnetic field. Fluid motions along magnetic field lines provide minimal resistance for isotropic velocity driving. Thus, as we discussed earlier, most energy is transferred this way. If the magnetic field were laminar, such motions could induce only acoustic-type turbulence. We disregard this possibility because acoustic turbulence does not exist within the incompressible limit we consider.

In the incompressible case, the structures created by the parallel fluid flow correspond to slow mode perturbations with the parallel magnetic field size L and perpendicular scale $LM_{\mathrm{A},b}$. These structures are sheared by the Alfvénic fluctuations discussed above. This transfers the scaling of weak Alfvén modes given by Equation (19) to slow modes but does not cascade the energy in the parallel direction.

In the case of fluid moving along a turbulent magnetic field that has the structure in the parallel direction, this structure gets imprinted to the flow. In other words, the magnetic field stochasticity is transferred to the stochasticity of the conducting fluid flow. As discussed in Section 2.1.3, strong Alfvénic turbulence introduces the structure in the parallel direction. Thus, following magnetic field lines, the velocity fluctuations reflect scaling of Alfvénic fluctuations parallel to the magnetic field, which (see Section 2.1.3) have the energy spectrum $k_\parallel^{-2}$. Therefore, the fluid flow along the magnetic field lines exhibits parallel fluctuations:

$$E_k \sim k^{-2}. \quad (19)$$

We expect this spectrum to change for $k > 1/LM_{\mathrm{A},b}$ because the strong MHD turbulence scaling dominates the spectrum at small scales. In particular, the fluid motions along magnetic field lines become a part of the pseudo-Alfvén cascade.

This stochastic fluid motion is not a part of MHD turbulence driven through magnetic fluctuations. It represents an additional element introduced by the velocity driving.

2.2.4. Scaling of Alfvénic Fluctuations

Magnetic field scaling in weak turbulence can present several regimes depending on the turbulence driving band. If the driving frequency band is "narrow," i.e., $\delta\omega \ll \omega_L$, the driving frequency ω_L will determine the principal frequency of parallel fluctuations in the numerical box. If the corresponding wavelength of the induced fluctuations V_{A}/ω_L is larger than the box size L, the large-scale magnetic fluctuations cannot be observed on the box size scale, naturally resulting in the dominance of the turbulent kinetic energy compared to the magnetic energy.

The situation is different if the driving frequency is "broad band." The critical scale for which the driving excites the Alfvénic perturbation that fits the numerical box corresponds to the wave frequency:

$$\omega_c = \omega_L \delta B/B. \quad (20)$$

For frequencies larger than ω_c, the turbulent cascade is Alfvénic, with kinetic and magnetic energies equal at such scales.

Injection coherence scale. As we mentioned in Section 2.2.1, for isotropic velocity driving, one can introduce the coherence scale corresponding to the perpendicular scale of the wavepackets. The velocity fluctuations injected at scale L propagate $LM_{\mathrm{A},b}$ perpendicular to the magnetic field. Thus, the perpendicular scale of fluctuations is limited by

$$L_{\perp,\max} \approx LM_{\mathrm{A},b}, \quad (21)$$

which corresponds to the perpendicular fluctuations arising from the largest scale driving. This corresponds to the upper boundary for the motions correlated perpendicularly. The cascade gets into a strong turbulence regime at the scale $l_{\mathrm{tr}} = LM_{\mathrm{A},b}^2$ at which the velocities and magnetic field are related through the Alfvén relation. According to Equation (3), the velocity amplitude at this scale is $V_L M_{\mathrm{A}}$. The increase of velocity and magnetic field fluctuations with the scale in the range $[l_{\mathrm{tr}}, L_{\perp,\max}]$ follows the weak MHD cascade given by Equation (17). Thus, the maximal amplitude of Alfvénic perturbations corresponds to

$$\delta B_{\max} \approx V_L \sqrt{4\pi\rho} M_{\mathrm{A},b}^{1/2}, \quad (22)$$

which suggests that the Alfvénic turbulence energy is $\sim M_{\mathrm{A},b}$ fraction of the kinetic turbulent energy. We will see further on that the amplitude $\delta B_{\max}$ corresponds to our earlier estimate of the magnetic fluctuation from Equation (12) if one accounts for Equation (28).

2.2.5. Scaling of Turbulence Fluctuations Parallel to Magnetic Field

Parallel to magnetic field fluctuations for incompressible flow are pseudo-Alfvén fluctuations, which are the limiting case of slow modes. The importance of slow modes for explaining unusual properties of sub-Alfvénic simulations was stressed by C. McKee (2024, private communication). These magnetic field compressions propagate with Alfvén speed V_{A} (see the Appendix).

Equation (9) describes the generation of pseudo-Alfvén modes by fluid flows along magnetic field lines. The shearing of pseudo-Alfvén fluctuations by the Alfvénic cascade is efficient when the Alfvén shearing rate $v_l/l_\perp$ becomes equal to the propagation rate of pseudo-Alfvén fluctuations over the injection scale, i.e., V_A/L. Equating the two, one gets the transition scale l_{tr} given by Equation (5). In other words, the cascading of pseudo-Alfvén fluctuations by Alfvénic cascade starts from perpendicular scale $LM_{A,b}^2$, which is smaller than the scale for the initiation of the Alfvén cascade through velocity driving by a factor $M_{A,b}$.

As we discussed earlier, in the case of velocity driving, the amplitude of pseudo-Alfvén fluctuations according to Equation (9) is $V_L M_{A,b}^{1/2}$. The direct nonlinear interaction of such fluctuations results in their cascading being slow. Thus, the pseudo-Alfvén fluctuations δB_s stay constant over the scales $[l_{tr}, L]$. The condition $\delta B_s \approx$ const results in the spectrum $\delta B_s \delta B_s \sim E_{B,s} k$ with scaling of the pseudo-Alfvén modes:[9]

$$E_{B,s}(k) \sim k^{-1}. \tag{23}$$

With velocity evolving according to Equation (18) and the magnetic energy evolving according to Equation (23), the difference between the two energies at the injection scale L amounts to

$$E_{B,s}(k_L) \approx E_k(k_L) M_{A,b}, \tag{24}$$

where $k_L \sim 1/L$, which demonstrates the self-consistency of our picture.

It follows from Equation (9) that the isotropic velocity driving is expected to induce the $\delta B_\perp \sim \delta B_\parallel$ at the scale of injection. Thus, we expect that

$$E_{B,s}(k_L) \approx E_{B,A}(k_L). \tag{25}$$

The Alfvénic cascading is expected to operate at the perpendicular scale $LM_{A,b}$. At the $LM_{A,b}^2$ scale, the amplitude of Alfvénic fluctuations is reduced by a factor $M_{A,b}^{1/2}$, which suggests the dominance of energy of pseudo-Alfvén/slow modes over Alfvén modes. A rough estimate of the relative amplitudes is

$$E_{B,A}(k) \approx E_{B,s}(k) M_{A,b}^{1/2}, \quad k > \frac{1}{l_{tr}}, \tag{26}$$

where $E_{B,A}$ is the spectrum of Alfvén modes and l_{tr} is given by Equation (5). Additional effects for $M_{A,b} < 1$ turbulence are related to the effect of accumulation of energy at the $k_\parallel = 0$ modes, which is frequently referred to by plasma turbulence community as "condensation" process (see A. A. Schekochihin et al. 2012). We consider these effects in a subsequent paper (K. H. Yuen et al. 2024, in preparation).

How stiff the magnetic field lines are in relation to the flow depends on the forcing scale and M_A. The magnetic field lines stay stiff for the motions $l_\parallel > l_\perp M_{A,b}^{-1}$. Such motions induced by the driving induce velocity fluctuations rather than magnetic fluctuations.

[9] In our next paper (K. H. Yuen et. al 2024, in preparation), we consider in detail the properties of the parallel and perpendicular spectra for these fluctuations for different types of driving.

2.3. Two Forms of Alfvén Mach Number

We note that the accepted textbook definition of the "velocity Alfvén Mach number" is the ratio of the turbulence injection velocity to the Alfvén one, i.e.,

$$M_A \equiv \frac{V_L}{V_A}. \tag{27}$$

Our study reveals that for the velocity-driven incompressible sub-Alfvénic turbulence, the kinetic energy exceeds the magnetic turbulent energy. Equation (24) corresponds to $\delta B^2 \sim \rho V_L^2 M_A^2$. By dividing both parts by V_A^2, we can see that the "magnetic Alfvén number" $M_{A,b}$ is related to the "velocity Alfvén number" M_A as

$$M_{A,b} = \frac{\delta B}{B} \approx M_A^2, \tag{28}$$

which is in contrast to the textbook definition given by Equation (1). The same result follows from dividing both parts of Equation (12) by B. The properties of the most important part of MHD turbulence, the Alfvénic cascade, depend on $M_{A,b}$, which is a fundamental number.

Note that the theory of MHD turbulence is traditionally formulated for incompressible fluid settings where only Alfvén and pseudo-Alfvén fluctuations are considered (see GS95). It is assumed that velocity fluctuations and magnetic field fluctuations are related through the Alfvén relation. However, as we showed, this is not the case for velocity-driven sub-Alfvénic turbulence (see Equation (12)).

Our paper deals with the properties of incompressible MHD turbulence. The fluid compressibility introduces an additional complexity. All three modes, Alfvén, slow, and fast, contribute to V_L for compressible MHD turbulence. The properties of turbulence depend on the relative contribution of the modes, apart from the value of V_L. This effect explains the difference in turbulence properties for solenoidal and potential driving obtained for the same M_A (see C. Federrath et al. 2008).

We note that the relation between $\delta B/B$ and M_A given by Equation (28) was reported in simulations (J. R. Beattie et al. 2020) and attributed to the effects of fluid compressibility. Similarly, by combining Equations (12) and (27), one can get the relation between kinetic and magnetic turbulent energies $E_B \approx E_k M_A^2$, which corresponds to the result established through the analysis of compressible numerical simulations (J. R. Beattie et al. 2022).[10] Our study suggests that, in fact, these effects arise from the velocity driving of MHD turbulence. We plan to numerically test this claim elsewhere but provide more physical arguments supporting our point in Section 6.3 and in the Appendix.

3. Numerical Simulations

In this study, we perform the incompressible MHD simulations with the pseudo-spectral code called MHDFlows.jl (K. W. Ho 2022).[11] MHDFlows is the newly developed MHD open-source code based on the dynamical language Julia with spectral solver framework FourierFlows.jl

[10] Another way to obtain this relation is to combine Equations (24) with (28).

[11] https://github.com/MHDFlows/MHDFlows.jl

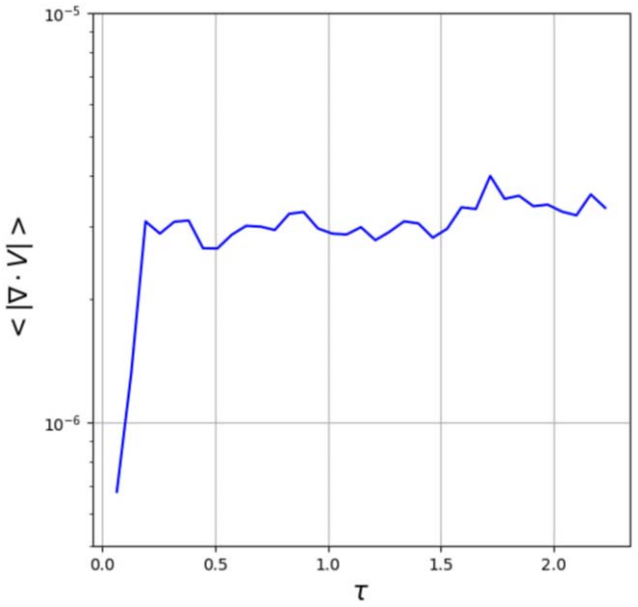

Figure 1. The absolute value of the compressible term in our code (Simulation used: M1).

(N. C. Constantinou et al. 2023). In contrast to the traditional spectral solver, it supports native GPU acceleration and supports wide ranges of MHD simulations, including ideal MHD, Electron-MHD, and MHD with volume penalization method. In this study, we solve the ideal MHD equation in the periodic box with the size of 2π:

$$\frac{\partial \boldsymbol{v}}{\partial t} + (\boldsymbol{v}\cdot\nabla)\boldsymbol{v} = -\nabla P + (\nabla\times\boldsymbol{B})\times\boldsymbol{B} + \nu\nabla^2\boldsymbol{v}$$
$$\frac{\partial \boldsymbol{B}}{\partial t} = \nabla\times(\boldsymbol{v}\times\boldsymbol{B}) + \mu\nabla^2\boldsymbol{B}. \quad (29)$$

All the symbols have their usual meaning. We use the method mentioned in J. Maron & P. Goldreich (2001), in which pressure P is chosen such that the equations maintain the divergence-free condition throughout the simulation. With these set up, we expect that both $\boldsymbol{B}$ and $\boldsymbol{v}$ will be incompressible over the course of the simulations. To illustrate this, Figure 1 demonstrates the evolution of the velocity divergence term. Its magnitude is maintained at the order of 10^{-6}, which is at machine accuracy (Float32) for this experiment. (Keep in mind that the incompressible velocity fluctuations are at the order of unity.) Uncertainties of such order cannot compromise the incompressible nature of our code to induce any noticeable effects on the time of our simulations. The turbulence is driven at large scale ($k = 1.5$) through the method proposed by K. Alvelius (1999). In addition, a guided field with different strengths was set up at the beginning of the simulation to control the M_A, and we analyzed the result after 10 large-scale eddy turnover times to wait for the saturation of kinetic and magnetic energies of turbulence. We use the Runge–Kutta method of order 4 (RK4) for the time integration and $2/3$ as the aliasing factor (see S. A. Orszag 1971). Table 1 shows the key parameters of our simulations. To characterize the magnetization of our simulations, we use the "velocity-based" definition of the Alfvén Mach number M_A given by Equation (27).

Table 1
Key Parameters of the MHD Incompressible Simulation That Will Be Used in This Paper

Simulation	$\langle M_A \rangle$
M0	0.393
M1	0.451
M2	0.588
M3	0.685
M4	0.825
M5	0.904
M6	0.906
M7	0.918
M8	1.041
M9	1.264

Note. $\langle M_A \rangle$ refers to the 10-slice time-averaged Alfvénic Mach number. The kinetic and magnetic diffusivities of the simulations are both 5×10^{-5}. The resolution of these simulations is 384^3. The magnetic Prandtl number is 1 for all simulations. The time-averaged Alfvénic Mach number is computed through the last five snapshots of each simulation.

4. Analysis of Numerical Results

4.1. Kinetic and Magnetic Energy of Turbulence

Figure 2 provides a visualization of our simulations corresponding to $M_A \approx 0.45$. The initial direction of the magnetic field is along the z-axis. The magnetic field and velocity are shown. In our incompressible MHD simulations with velocity driving, we observe that the amplitude of velocity fluctuations exceeds those of the magnetic field.[12] We also observe that the magnetic field is more structured than velocity. This indicates a more shallow energy spectrum of the magnetic field at the scales close to the injection scale. Statistically, this alignment is preserved in the driving process, but different realizations that we analyze exhibit the deviations of the mean field from its initial direction.

Figure 3 shows the spectra of the magnetic field and velocities for different M_A. The magnetic field spectrum for large scales is consistent with the predicted magnetic energy spectrum $E_B \sim k^{-1}$ (see Equation (23)), while the kinetic energy spectrum corresponds to $E_k \sim k^{-2}$, which agrees with our prediction given by Equation (19).

The convergence of the spectra around the value l_{tr} is observed. As the M_A increases, the difference between the magnetic and velocity spectra decreases, as shown in Figure 3, with two spectra merging toward the GS95 incompressible turbulence spectrum corresponding to $M_A = 1$. On the contrary, as M_A decreases, the difference between the velocity and magnetic field spectra gets more prominent. Figure 3 shows the spectra for $M_A \approx 0.09$. For such low M_A, turbulence reaches

[12] We note, parenthetically, that a similar difference was observed in earlier numerical studies of compressible MHD turbulence (J. R. Beattie et al. 2022; R. Skalidis et al. 2023b) that also employed velocity driving. This suggests that the disparity in magnetic and velocity turbulent energies arises from velocity driving and is not related to fluid compressibility.

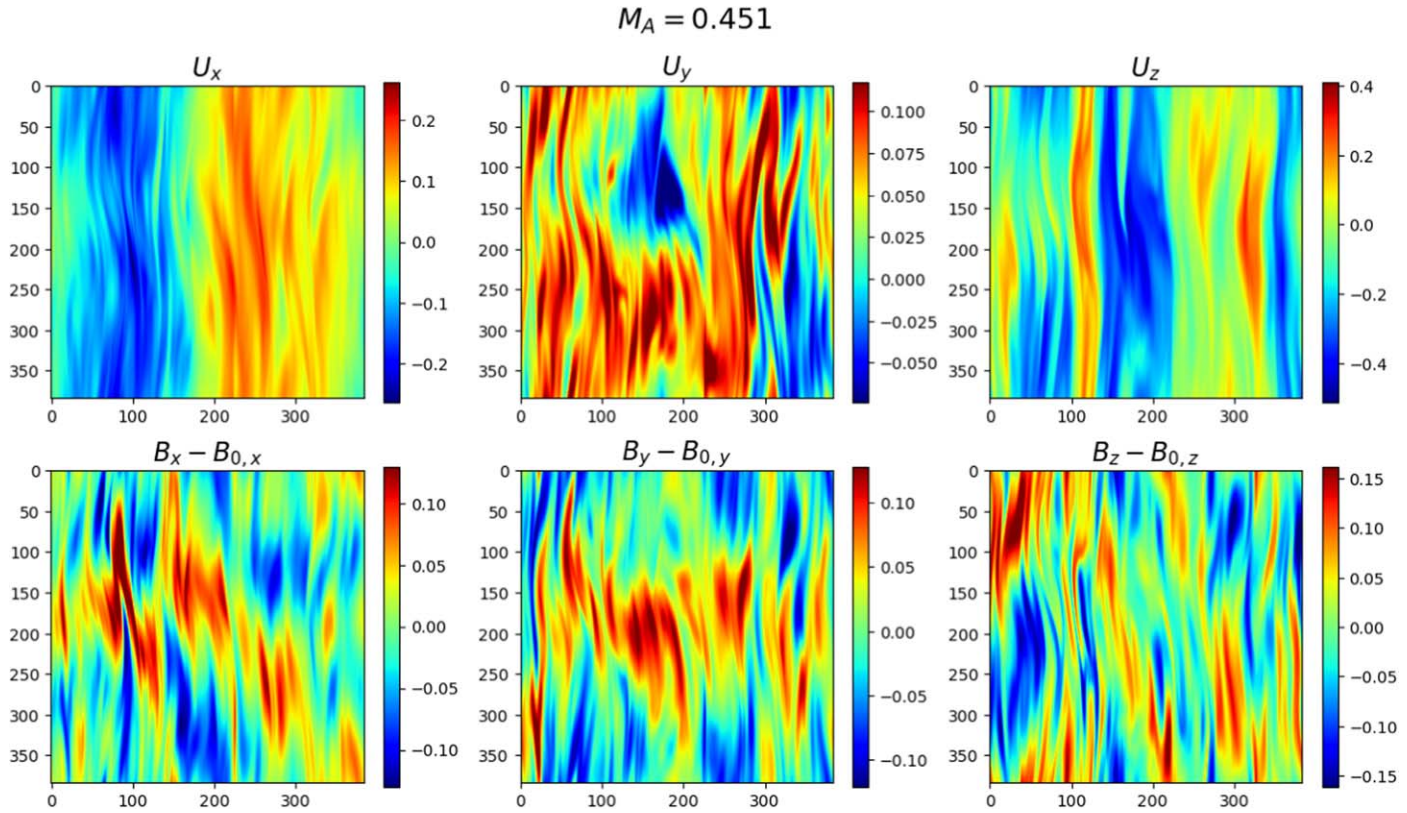

Figure 2. A 2D slice of simulations with $M_A \approx 0.45$. The mean field directed along the z-axis was subtracted to focus on fluctuations. The upper panels are velocity components, the lower panels are the components of magnetic fluctuations.

the dissipation scale before its transfer to the strong MHD turbulence regime.

To test whether the disparity of magnetic and kinetic energies arises from the way we drive turbulence, in Figure 4 we provide spectra of sub-Alfvénic turbulence driven by magnetic fluctuations. In this case, we observe that $E_k = E_B$ corresponds to our theoretical expectations.

To test to the effect of the resolution, we also perform a convergence test of the magnetic spectrum with different resolutions in Figure 5, showing spectra converged for all resolutions. We realize that to establish the exact spectral slope numerically, one requires a separate dedicated study. Thus, we cautiously use "consistent" to describe our numerical results.

4.2. Parallel and Perpendicular Fluctuations

The kinetic and magnetic energy spectra measurements do not capture the difference between the motions along and perpendicular to the magnetic field. Such measurements must be done with respect to the magnetic field's local direction. Therefore, the spectra measured in the frame of the mean magnetic field are not sufficiently informative. To deal with this problem, we employ the second-order structure functions measured with respect to the local magnetic field for our study (see J. Cho & E. T. Vishniac 2000). For such measurements, the magnetic field of the magnetized eddy defines the reference frame.

To stress that the measurements are done in the local system of reference in Figure 6, we use the word "local" in front of structure functions of magnetic and velocity fields. Figure 6 demonstrates that both the fluctuations of the magnetic field and the velocities are elongated along the magnetic field direction, but their anisotropy is very different. This is a clear distinction from the strong MHD turbulence, where the velocities and magnetic field exhibit the same scaling, as discussed earlier. In the sub-Alfvénic velocity-driven case that we consider, the anisotropy of velocities is more prominent compared to the magnetic fluctuations. We expect this effect to be slightly mitigated in compressible simulations due to the presence of fast modes. Note that the strong anisotropy of velocity fluctuations is observed in compressible turbulence simulations in X.-N. Bai (2022) for $M \ll 1$. The velocity structure functions are strongly correlated with the direction of the magnetic field due to the fluid flowing along the magnetic field.

We show both structure functions corresponding parallel fluctuations, i.e., $SF_{2B}(k_\parallel = 0)$ and $SF_{2V}(k_\parallel = 0)$, as well as perpendicular fluctuations, i.e., $SF_{2B}(k_\perp = 0)$ and $SF_{2V}(k_\perp = 0)$. We only use $k_\perp$ and $k_\parallel$ as shortcut convenient notations. The measurement is done in the local system of reference, which differs, in general, from the mean-field magnetic field reference frame. The results are strikingly different for small M_A, indicating the different physics of motions parallel and perpendicular to the magnetic field.

The energy of magnetic compressions corresponding to pseudo-Alfvén modes (see J. Cho & A. Lazarian 2003) is subdominant at large scales compared to kinetic energy.

For small M_A, the amplitude of velocity fluctuations parallel to the magnetic field significantly exceeds the one perpendicular to the magnetic field. The latter is similar to the amplitude of magnetic fluctuations in the units of Alfvén

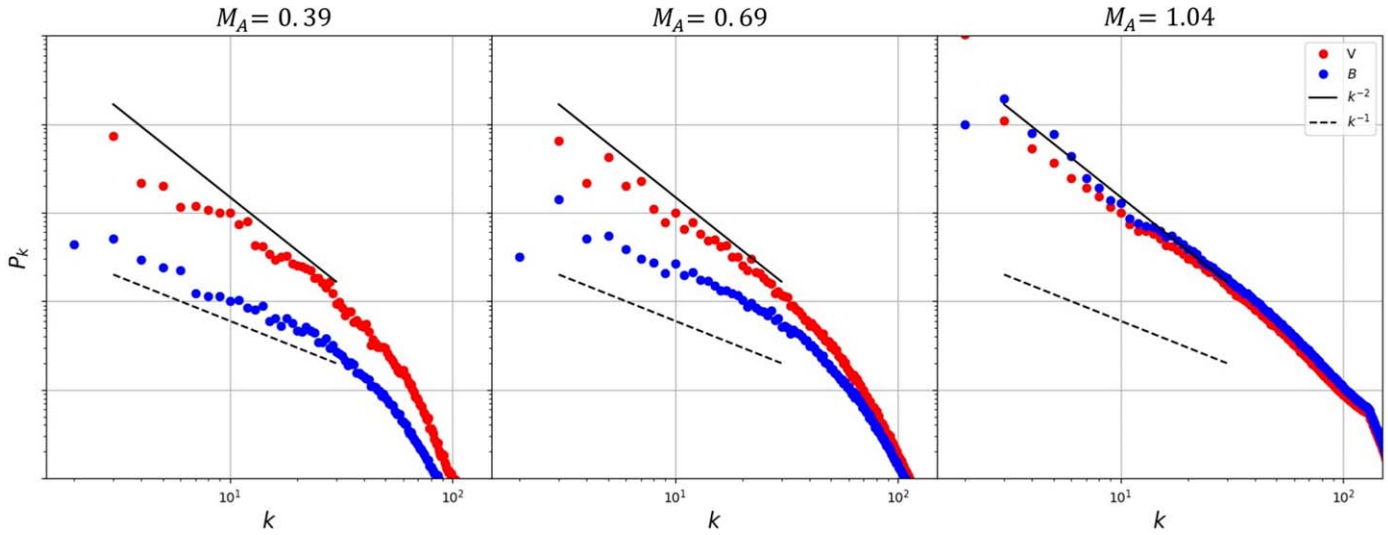

Figure 3. Velocity and magnetic field spectra for different $\delta B/B$, showing the change of magnetic spectra. The disparity between magnetic and velocity turbulent energies is large for small M_A. When magnetic fluctuations become of the order of unity, the disparity between kinetic and magnetic energy disappears. The solid and dashed lines correspond to the theoretical expectations for velocity and magnetic spectra for sub-Alfvénic turbulence given by Equations (19) and (23).

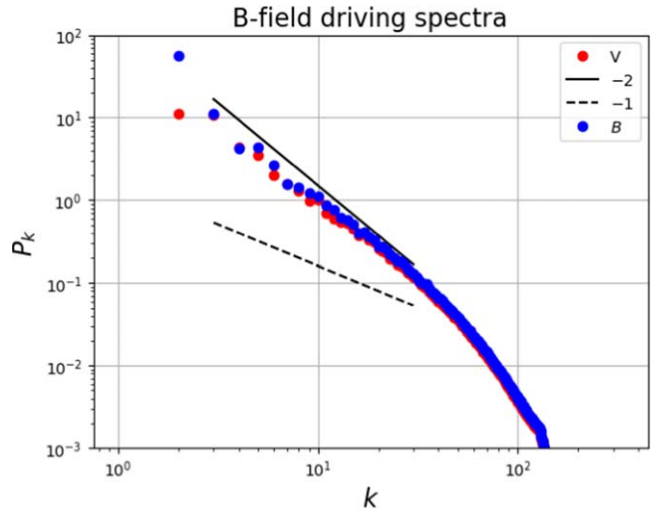

Figure 4. Energy spectra for both velocity and magnetic field with magnetic field driving of sub-Alfvénic turbulence, with $M_A = 0.7$. In contrast with the velocity driving, the magnetic and kinetic energies are at equipartition.

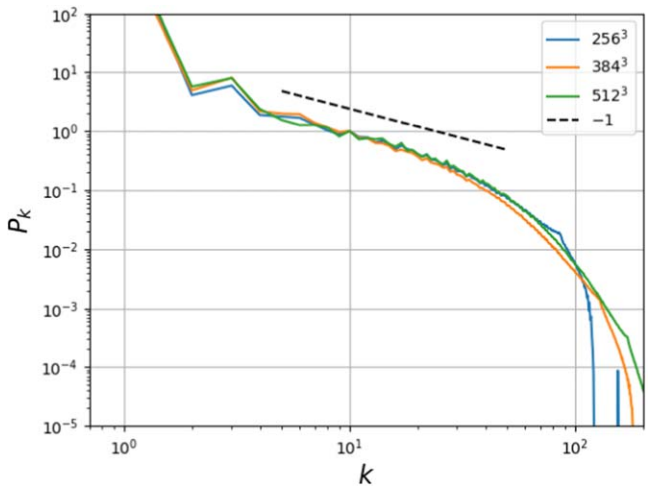

Figure 5. A comparison of magnetic spectra obtained with different resolutions using the setting of M3 corresponding to $M_A \approx 0.28$. The spectrum $E_B \sim k^{-1}$ corresponding to $\delta B = \text{const}$ is shown by a dashed line.

velocity, indicating that the fluctuations perpendicular to the magnetic field are connected by the Alfvén relation. In contrast, the amplitude of velocity fluctuations is larger than that of the magnetic fluctuations in Alfvén velocity units, demonstrating that velocity fluctuations along the magnetic field dominate. We associate those with flows along magnetic field lines induced by velocity driving. This effect is absent for the magnetic driving of sub-Alfvénic turbulence.

Another significant effect illustrated by Figure 6 is the higher amplitude of pseudo-Alfvénic fluctuations, compared to Alfvén fluctuations at small scales. The amplitude of the fluctuations is similar at the injection scale. Still, the compressible fluctuations marginally change their amplitude at large scales, while the Alfvénic perturbations follow the turbulent cascade for all scales. This corresponds to our expectations in Section 2.2. As we discuss later, this newly identified effect has astrophysical significance.

4.3. Simulations of Synthetic Observations for Two Ways of Driving

There is a significant difference between the results obtained with magnetic and velocity driving of turbulence. We provide the synthetic observations of magnetically and velocity-driven (Figure 7) MHD cubes to test how to distinguish the two cases from observations. In observations, the parallel velocity fluctuations can be obtained from Doppler-shifted spectral lines using velocity centroids, while the plane-of-sky magnetic field fluctuations can be obtained using polarization direction fluctuations (see A. Lazarian et al. 2022). We provide the results corresponding to the analysis of the data corresponding to $k_{\|,G} = 0$ Fourier component harmonic. The subscript "G" denotes the measurements taken in the global mean-field system of reference. This is the only system of reference available in observational studies.

A comparison between panels of Figure 7 reveals that for velocity-driven turbulence, the structure function of velocity

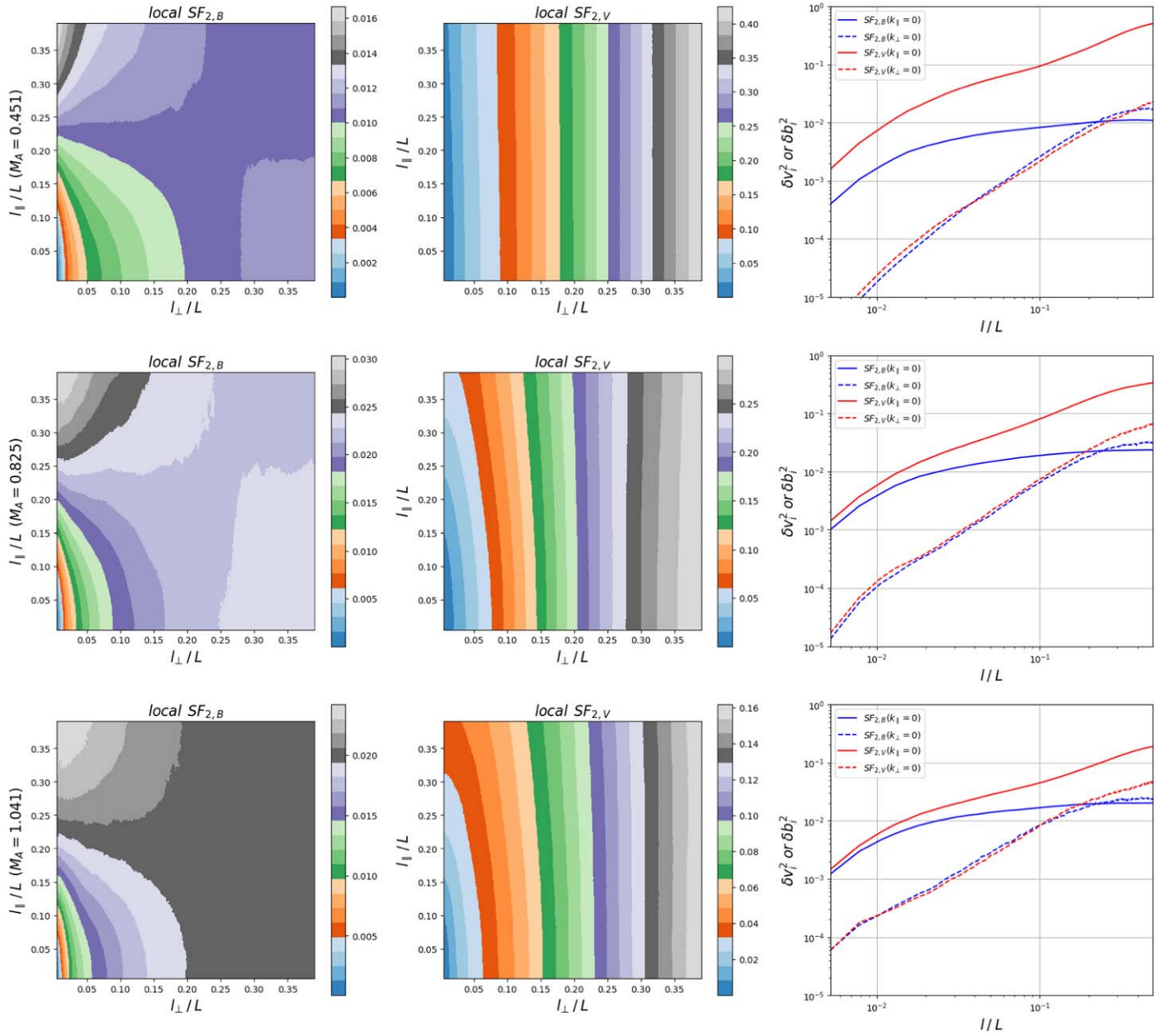

Figure 6. Left panels: contours of the second-order local structure function of magnetic field $SF_{2,B}$, Middle panels: Contours of the second-order local structure function of velocity field $SF_{2,V}$. Right panels: variation of local parallel and perpendicular structure functions for different M_A. The dominance of parallel velocity fluctuations increases with the decrease of M_A.

parallel to mean magnetic field is significantly larger than the structure function of velocities measured perpendicular to the magnetic field. On the contrary, the two functions converge at large scales for magnetically driven turbulence. This opens the way to observationally distinguish between the two cases. We will explore this in a future study.

5. Comparison with the Earlier Studies of Sub-Alfvénic Turbulence

5.1. Velocity Driving Providing $E_B = E_k$

Studies of diffusion induced by sub-Alfvénic turbulence were undertaken in R. Santos-Lima et al. (2021). Since elongated boxes and anisotropic driving were employed in these studies, the results are difficult to compare with those in this paper. In particular, the equipartition between the kinetic and magnetic energies was reported, i.e.,

$$E_{\mathrm{weak},k} = E_{\mathrm{weak},m}, \tag{30}$$

which we attribute to the anisotropic driving that was intended to prevent the excitation of modes with $k_\parallel = 0$.

The driving in R. Santos-Lima et al. (2021) is rather special. We doubt that this type of restricted driving is common in typical astrophysical environments. More research is required to answer this question. Our study shows that, unlike trans-Alfvénic turbulence, sub-Alfvénic turbulence is more sensitive to the properties of the large-scale turbulence driving.

Note that while simulations in R. Santos-Lima et al. (2021) confirmed the dependencies of the reconnection diffusion obtained for weak turbulence in A. Lazarian (2005), the

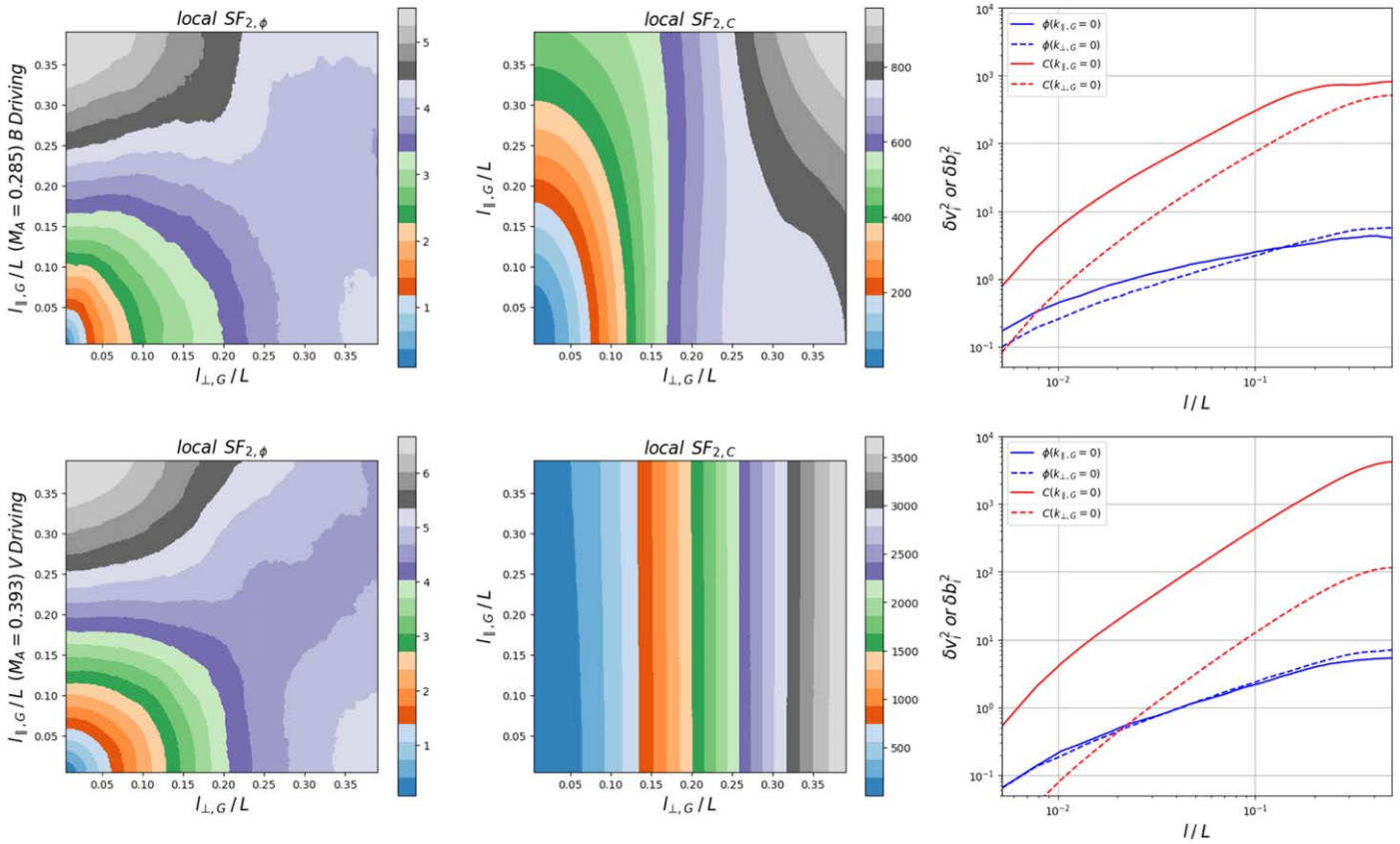

Figure 7. Structure functions and contours of equal correlation perpendicular to the line-of-sight magnetic fluctuations and parallel to the line-of-sight velocity fluctuations corresponding to $k_\parallel = 0$. Left panels: contours of equal correlation for the POS magnetic field fluctuations. Middle panels: contours of equal correlations for velocity centroids. Right panels: structure functions of the POS magnetic field that can be measured through polarimetry and structure functions of velocity centroids available through observations. Upper row: magnetically driven case. Lower row: the same as in the upper panel, but for the velocity-driven case.

turbulence scaling reported did not agree with all the predictions of the classical weak turbulence theory (see S. Nazarenko 2007).

5.2. *Velocity Driving Providing* $E_B/E_k = M_{A,b}$

The discussion of the disparity of kinetic and magnetic energies in compressible turbulence can be traced back to C. Federrath et al. (2016), where for $B_0 \gg \delta B$ the magnetic energy was presented as

$$B^2 \approx (B_0 + \delta B_\parallel)^2 + \delta B_\perp^2 \approx B_0^2 + 2B_0\delta B_\parallel, \quad (31)$$

and the second term, $B_0\delta B_\parallel$, was identified with the turbulent part of the magnetic energy and equated to the kinetic energy[13]

$$\langle B_0\delta B_\parallel\rangle \approx \langle \rho\delta V_L^2\rangle, \quad (32)$$

where the $\langle ...\rangle$ denote ensemble averaging and the V_L is the injection speed in compressible MHD simulations. P. S. Li et al. (2022) stated that identifying $B_0\delta B_\parallel$ with magnetic energy is unjustified, which agrees with the conclusion in J. Liu et al. (2022). It is easy to see that Equation (32) and our Equation (9) differ radically. They differ in the underlying physics, assumptions made during the derivation, and their final form. In particular, our derivation suggests that $|\delta B|$ is the standard deviation of magnetic fluctuation in contrast with the fluctuation of magnetic field, i.e., a random variable with zero mean, that enters Equation (32).

The original derivation of Equation (32) was reproduced in ST21, but later publications attempted to ensure that the left-hand side of the equation is positively defined, i.e., $\langle\delta B\rangle \stackrel{!}{=} \sqrt{\langle\delta B^2\rangle}$, because this was required to make $B_0\delta B_\parallel$ the dominant part of the fluctuation of magnetic energy. These attempts include the introduction of two different potentials that govern parallel and perpendicular fluctuations of the magnetic field in R. Skalidis et al. (2021). The authors claim that harmonic oscillations of δB making the $\langle B_0\delta B_\parallel\rangle$ equal to zero are present in the case of incompressible turbulence, but for "compressible strongly magnetized turbulence" the oscillator is not harmonic, and the "potential energy of perturbations (here of the magnetic field) is linear, $\delta\epsilon_{p,\mathrm{compressible}} \propto \delta B$" rather than to $(\delta B)^2$. However, this conclusion follows from the authors' assumption routed in Equation (32) rather than an outcome of calculations that were supposed to result in the potential proportional to δB^2 after applying the accepted averaging procedure. It is also surprising why $\delta B_\parallel$ and $\delta B\perp$, according to simulations, stay within a factor of 2 for a wide range of $M_A < 1$, despite being governed by potentials of different natures. In contrast, the correspondence of parallel and perpendicular magnetic fluctuations expressed by Equation (11) is straightforward in our derivation.

If one first takes squares of both parts of Equation (32) and then performs averaging, formally, the problem on the left-

[13] This involves redefining what turbulent magnetic energy is and disagrees with the fact that the velocity-driven sub-Alfvénic turbulence has an excess of kinetic energy over magnetic energy.

hand side of the resulting equation stops being zero. This was suggested in J. R. Beattie et al. (2022; henceforth BX22), where it was proposed to consider the "second moment of the energy balance equations." Such a physical quantity had never been used in classical mechanics and its physical meaning/significance was unclear, as pointed out in A. Lazarian et al. (2022). In other words, while solving some problems, this approach created new questions.

Finally, a sophisticated approach involving Lagrangian description of compressible MHD turbulence was suggested in R. Skalidis et al. (2023b). The authors conclude that "for sub-Alfvénic and compressible turbulence, we find that $\boldsymbol{B}_0\delta\boldsymbol{B}$ is the leading term in the dynamics, and as a result, the scaling of the velocity and magnetic fluctuations become $\delta u_l \sim \sqrt{B_0\delta B_l}$, or equivalently, $M_A \sim \delta u_l/V_A \sim \sqrt{\delta B_l/B_0}$." The former expression corresponds to the relation that follows from Equation (32), provided that δB is positively defined. The authors stress, that in their formalism, "the incompressible limit is approximated when $\boldsymbol{B}_0\delta\boldsymbol{B} = 0$." This means that Equation (28) and related Equation (24) should not be true in the incompressible case. This contradicts the results in this paper. We suspect that the authors do not account for the fact that slow modes compress the magnetic field even if the fluid is incompressible

All of the studies above assume that turbulence compressibility is mandatory for obtaining the relations that we, nevertheless, obtained for incompressible sub-Alfvénic turbulence. At the same time, none of the earlier studies suspected that the velocity driving induces the effects we reported in the present paper.[14] We reiterate in Equation (9) that $|\delta B|$ is the standard deviation of magnetic fluctuation rather than the random variable with zero mean, as it is in Equation (32). This follows from our derivation and does not require an additional hypothesis.

For the sake of completeness, below we mention other differences with the earlier studies of properties of sub-Alfvénic turbulence. BX22 stresses the difference in their results from the classical theory of sub-Alfvénic turbulence and conjectures that sub-Alfvénic turbulent fields may not exist for $M_A < 2$. Our results contradict the latter hypothesis. This paper predicts and demonstrates through numerical testing a well-defined turbulent scaling. Our study shows that the turbulent description of random velocities applies to magnetized fluids with a high Reynolds number at any M_A.

In addition, the aforementioned studies associate the differences in the outcome of their simulations and the classical MHD theory (e.g., GS95) with the effects of compressibility. For instance, they report that fluid compressibility causes the dominance of kinetic energy over magnetic turbulent energy in $M_A < 1$ simulations (see ST21; R. Skalidis et al. 2021). On the contrary, our study deals with incompressible turbulence and gets the same relations between E_k and E_B. Formally, the latter does not disprove the former but shows that compressibility cannot be the sole agent responsible for the energy disparity. The striking similarity of the results obtained in the presence and absence of compressibility presents a problem for the earlier theories. We hypothesize that in both cases the driving is the cause of the disparity. Our hypothesis can be tested by simulating compressible turbulence with magnetic driving. If our hypothesis is correct, we will not see a significant disparity between turbulent magnetic and kinetic energies for magnetically driven turbulence. However, such a study is beyond the scope of the present work, which is focused on the fundamental properties of incompressible sub-Alfvénic turbulence.

[14] We note parenthetically that in the aforementioned papers Equation (32) is assumed to be true for any choice of ensemble volume. In the language of turbulence, this means that Equation (32) holds for all choices of wavenumber k. This is different from our derivation of Equation (9), where we consider the pressure balance only at the injection scale. In the case of compressible supersonic turbulence, the scalings of $\delta\rho$, δv, and δB are different (G. Kowal & A. Lazarian 2010) and the energy conservation arguments may not hold for individual modes.

5.3. Magnetically Driven Turbulence with $E_B = E_k$

If chaotic magnetic field motions drive turbulence, kinetic energy does not exceed magnetic energy. Thus, even for $M_A < 1$, the turbulence is expected to be in the strong MHD regime at all scales. This was noted in G. Eyink et al. (2013) in relation to turbulence arising from turbulent reconnection (see also A. Lazarian et al. 2020). For strong Alfvénic turbulence,

$$E_k = E_B \tag{33}$$

for every scale, starting from the injection scale. An example of how the equipartition is reemerged is shown in Figure 4, where we drive the turbulence mathematically similarly to the kinetic counterpart from the induction equation instead of the momentum equation.

The physical reasoning of why a violation of equipartition is not observed in this case is rather trivial. The cascade time (Equation (15)) given by the small velocity fluctuations transferred from the magnetic field driving is significantly longer than both timescales (see Section 2.2.2) of weak turbulence. As a result, the system has enough time to develop itself to the equipartition state before hitting the cascade time boundary as outlined in Section 2.2.2.

Turbulence induced by magnetic reconnection is an example of this type of turbulence (see numerical simulations of this front; e.g., G. Eyink et al. 2013; G. Kowal et al. 2017; L. Yang et al. 2020).

This type of sub-Alfvénic turbulence is another example of the way that the excitation of turbulence affects its properties. The driving of sub-Alfvénic turbulence in terms of Elsässer variables is frequent in numerical simulations (see A. Beresnyak & A. Lazarian 2019). This driving is similar to the magnetic driving of turbulence. Instabilities related to the magnetic field are expected to provide magnetic driving (see more from Section 8.3).

6. Properties of Magnetic Fluctuations

6.1. Comparison with Theoretical Expectations: GS95 and LV99

The study in GS95 was performed for trans-Alfvénic turbulence. Our results smoothly transfer to this regime as $M_A \to 1$.

The analytical scaling that involves the Alfvén Mach number was introduced in LV99. It was extensively used in subsequent publications to describe different physical processes, e.g., the propagation of cosmic rays (see H. Yan & A. Lazarian 2002, 2003, 2008; V. Petrosian et al. 2006; S. Xu & H. Yan 2013; S. Xu & A. Lazarian 2016; M. R. Krumholz et al. 2020; Y. Hu et al. 2022a; S. Maiti et al. 2022) and damping of streaming instability by MHD turbulence (see A. Lazarian 2016; F. Holguin et al. 2019; P. F. Hopkins et al. 2021; X.-

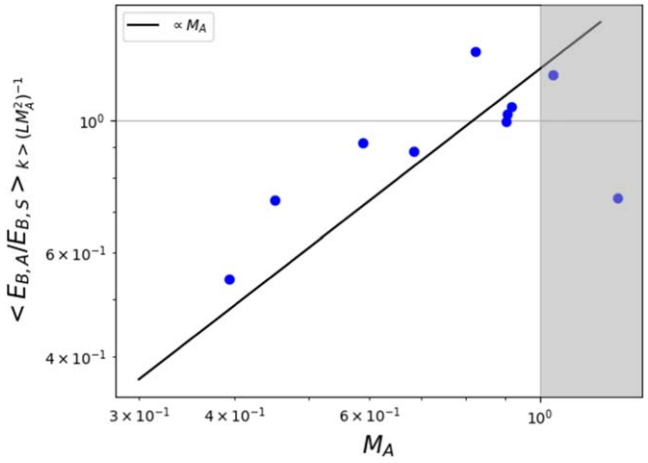

Figure 8. The relation of the mean magnetic spectra ratio of slow and Alfvénic modes for the strong turbulence regime. The gray region represents the region that is super-Alfvénic.

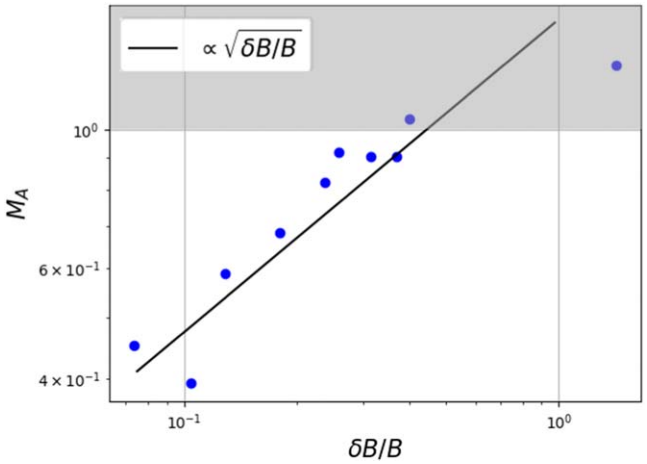

Figure 9. Scaling of $M_{A,b} = \delta B/B$ with the traditional Alfvén Mach number M_A for our simulations in Tab.1. The gray region represents the super-Alfvénic domain.

N. Bai 2022; A. Lazarian & S. Xu 2022; S. Xu & A. Lazarian 2022).

These results stay intact for the magnetic driving of sub-Alfvénic turbulence. However, for the velocity driving of turbulence, $M_{A,b}$ should be used to describe the dynamics of Alfvénic part of the cascade.

6.2. Comparison with Trans-Alfvénic Numerical Studies: J. Cho & A. Lazarian (2003)

Numerical decomposition of MHD turbulence into slow, fast and Alfvén modes was performed in J. Cho & A. Lazarian (2003) and, with modifications, in the subsequent publications (see G. Kowal & A. Lazarian 2010; A. Beresnyak & A. Lazarian 2019; K. D. Makwana & H. Yan 2020; K. W. Ho & A. Lazarian 2021, 2023; Y. Hu et al. 2022a; K. H. Yuen et al. 2023; P. Pavaskar et al. 2024). This study uses the original J. Cho & A. Lazarian (2003) approach to explore how energy partition between the modes proceeds in sub-Alfvénic turbulence. We deal only with Alfvén and slow/pseudo-Alfvén modes for incompressible turbulence.

We argued above that for the velocity driving of sub-Alfvénic turbulence, the energy of slow modes is expected to exceed the energy of Alfvén modes in the regime of strong MHD turbulence. The corresponding testing is presented in Figure 8. This result is consistent with Figure 6, which shows that the cascading of Alfvén and slow modes starts at different scales.

In earlier studies, it was assumed that MHD turbulence properties do not depend on whether the turbulence is driven by magnetic or velocity fluctuations.

The results of Figure 8 are different from the results in J. Cho & A. Lazarian (2003), where for trans-Alfvénic turbulence, the energies of slow and Alfvén modes were found to be of the same order. However, our present study shows that for velocity driving of MHD turbulence, this is only true for the case of $M_A \approx 1$.

The dominance of velocity fluctuations in sub-Alfvénic turbulence entails many astrophysical consequences missed through extrapolating results in J. Cho & A. Lazarian (2003) to the sub-Alfvénic regime. We mention some consequences in Section 8.

6.3. Comparison with Sub-Alfvénic Compressible Numerical Simulations: J. R. Beattie et al. (2020)

In Section 2.3, we argued that for the case of incompressible MHD turbulence driven by velocity fluctuations, the normalized magnetic field fluctuation $\delta B/B$ scales as the squared Alfvén Mach number M_A. This expectation is confirmed by Figure 9 for our incompressible simulations.

In their study of compressible MHD turbulence, J. R. Beattie et al. (2020) obtained a similar relation. This correspondence between results obtained for the compressible and incompressible cases may be suggestive that for velocity-driven MHD turbulence, the fluid flow along the magnetic field lines dominates the velocity dispersion and induces magnetic fluctuations in a way that marginally depends on fluid compressibility. This hypothesis should be tested by future research. Below, we provide a few considerations related to what one may expect due to the effects of compressibility.

The major difference between compressible and incompressible MHD turbulence is the absence of fast modes in the incompressible case. In addition, incompressible turbulence formally corresponds to the infinitely large ratio of the sound to Alfvén speed, i.e., to $\beta = \infty$. For $\beta < 1$, the nature of slow modes also changes compared to the high β case (J. Cho & A. Lazarian 2002). The magnetic fluctuations induced by fluid flow along the magnetic field lines (see Section 2.2.1) in low-β cases induce fast modes. Finally, compressible driving employed in J. R. Beattie et al. (2020) changes the ratio between energies of slow, fast, and Alfvén modes (S. Maiti et al. 2022). All these effects are expected to alter the relations between the dispersions of magnetic and velocity fluctuations. The fact that Equation (28) holds for the compressible settings explored in J. R. Beattie et al. (2020) indicates the subdominance of these effects for the velocity-magnetic field relation at the injection scales.

To what extent the results we obtained for an incompressible turbulence case, i.e., for turbulence in media with $\beta = \infty$ and sonic Mach number M_s equal 0, can be modified for a wide range of astrophysically relevant β and M_s requires further studies. One can argue that our considerations in Section 2.2.1 do not directly depend on the media β. For instance, for sub-Alfvénic turbulence, the low-β fluid flow generated by random velocity driving will align with the magnetic field and the

fluctuations of velocity will create pressure fluctuations that will induce $\delta B_{\parallel}$ according to Equation (9). This, in turn, will induce the perpendicular fluctuations given by Equation (12) due to a divergence-free constraint on the magnetic field. Similarly, if the fluid motions along magnetic field lines dominate at the driving scale, the velocity dispersions should not be much affected by shocks accompanying turbulence in high sonic Mach number media.

Some astrophysical media are not isothermal. We expect to see different statistics in this case. For instance, it is reported that in the case of multiphase media, fast mode generations are far more efficient and can arrive up to 50% of the total turbulence energy due to thermal instability (A. Beresnyak et al. 2024, in preparation; see also K. W. Ho et al. 2023, 2024a, 2024b).

Naturally, the difference between $M_{\rm A}$ and $M_{{\rm A},b}$ disappears for the incompressible MHD turbulence if turbulence is driven, e.g., in terms of Elsässer variables or driven by magnetic fluctuations, as follows from Figure 4. These two Alfvén Mach numbers can be somewhat different if magnetic fluctuations drive compressible turbulence. The value and importance of this difference should be established through further research.

Our present study is not limited to establishing the relations between the dispersions of turbulent magnetic fields and velocities. Equation (26) establishes that the velocity driving in high-β fluid induces the dominance of slow modes over the entire turbulence inertial range.

7. Implications for Techniques in Estimating Magnetic Field Strength

7.1. Davis–Chandrasekhar–Fermi Technique for Turbulence with $\mathrm{E_B} = \mathrm{E_K}$

Magnetic field strength measurements are important but challenging (see R. M. Crutcher et al. 2010). Tracing variations of magnetic field $\delta B_{\perp}$ measured by dust polarization (B. G. Andersson et al. 2015) and combining those with the measures reflecting the velocity fluctuations provides a valuable way of estimating plane-of-sky (POS) magnetic field strength in astrophysical settings. The resulting expressions depend on how the fluctuation of $\delta B_{\perp}$ and the measures of velocity fluctuations are related.

The roots of combining dispersions of magnetic field $\delta\phi$ with line-of-sight dispersion of velocity δv measured through spectroscopic observations to find the magnetic field strength in molecular clouds can be traced to the pioneering studies by L. Davis (1951) and S. Chandrasekhar & E. Fermi (1953). We refer to the original studies and their subsequent modifications/improvements that employ $\delta\phi$ and δv to estimate the magnetic field B as the DCF technique.

For small perturbations, the fluctuations of the POS magnetic field direction are

$$\delta\phi \approx \frac{\delta B_{\perp}}{B}, \tag{34}$$

Within the DCF technique, magnetic fluctuations arise from Alfvén waves with amplitude $\delta B = \sqrt{4\pi\rho}\,\delta v$. This results in $\delta\phi \approx \sqrt{4\pi\rho}\,\delta v/B$, which for angle $\gamma = \pi/2$ between the line of sight and the mean magnetic field provides the well-known DCF expression:

$$B_{\perp} \approx f\sqrt{4\pi\rho}\,\frac{\delta v}{\delta\phi}, \tag{35}$$

where f is a factor that is empirically adjusted to account for the complexity of the realistic settings compared to the DCF model.

With the advances in our understanding of interstellar medium dynamics (see C. F. McKee & E. C. Ostriker 2007), we now understand that the relations between $\delta\phi$ and δv should be obtained via employing MHD turbulence theory.

A closer look at Equation (35) suggests that the variations of dust polarization reflect the variations of the magnetic field direction perpendicular to the line of sight, i.e., $B_{\perp}$, while the Doppler broadening is affected by the fluctuations of the line-of-sight components of turbulence velocities, i.e., $\delta v_{\parallel}$.[15] In Alfvénic turbulence, the velocity fluctuations are perpendicular to that of the magnetic field, which induces the dependence of factor f on the angle γ between the 3D direction of the magnetic field and the line of sight. Accounting for the existence of slow and fast modes in MHD turbulence (GS95, Y. Lithwick & P. Goldreich 2001; J. Cho & A. Lazarian 2003), makes f dependent on γ and the relative contribution of fundamental modes into MHD turbulence. For the magnetically driven turbulence, one can write

$$B_{\perp} \approx f_1(\gamma)\sqrt{4\pi\rho}\,\frac{\delta v_{\parallel}}{\delta\phi}, \tag{36}$$

where the velocity dispersion is measured parallel to the line of sight and the angle dispersion is measured perpendicular to the line of sight.

Historically, the dependence of $f_1(\gamma)$ on γ is not given enough attention with most of the numerical studies focused on $\gamma = \pi/2$ case. This is an omission, which is crucial to correct while studying anisotropic sub-Alfvénic turbulence, as this paper demonstrates.

A simplification comes from the fact that $\delta\phi$ is dominated by the Alfvénic modes (LV99). However, other modes contribute to $\delta v_{\parallel}$. This makes the functional dependence of $f(\gamma)$ nontrivial, even in the most studied case of B-driving of turbulence—see K. H. Yuen et al. (2023) and S. Malik et al. (2023) for a method of obtaining γ, and S. Malik et al. (2024) for an application.

7.2. DCF for Turbulence with Equipartition Violated

We note that Equation (36) relies on the general equipartition of magnetic and kinetic turbulent energies, which should not be taken for granted according to the present paper.

The earlier researchers touched upon the importance of turbulence compressibility (see E. C. Ostriker 2003) for DCF. Our study shows that the outcome depends much more on the turbulence driving.

As we discussed earlier, the equipartition between turbulent magnetic and kinetic energies is strongly violated at $M_{\rm A} \ll 1$. Thus, Equation (36) must be modified to account for the modification of turbulence.

[15] To justify DCF approach, one should assume that the magnetic and velocity fluctuations arise from the same magnetized motions. Assuming turbulence isotropy, the technique relates the polarization measures perpendicular to the line-of-sight magnetic field fluctuations, i.e., $\delta B_{\perp}$, with the Doppler broadening providing the line-of-sight fluctuations $\delta v_{\parallel}$.

In the case of velocity driving, the fluctuation of the magnetic field direction given by Equation (34) is related to M_A via Equation (28). Combining this with the definition of the velocity Alfvén Mach number given by Equation (27), one can easily get the modified DCF expression:

$$B_\perp \approx f_2(\gamma)\sqrt{4\pi\rho}\,\frac{\delta v}{(\delta\phi)^{1/2}}, \tag{37}$$

where $f_2(\gamma)$ is another factor that depends on the direction of the magnetic field and the angle between the mean magnetic field and the line of sight. In general, $f_2(\gamma)$ is different from $f_1(\gamma)$ and both factors should be determined through dedicated studies similar to the one in A. Lazarian et al. (2022).

Equation (37) was first suggested in ST21 as a substitute for the DCF equation for compressible MHD turbulence, as opposed to the incompressible MHD turbulence that we deal with in this paper. Their approach was termed in P. S. Li et al. (2022) the "parallel-δB version of DCF" because the derivation was based on Equation (32), which involves only the parallel component of magnetic fluctuation $\delta B_\parallel$ (see also R. Skalidis et al. 2023b). As discussed earlier, Equation (32) includes averaging, which makes the left-hand side of the equation zero by the very definition of the magnetic field fluctuation. Apart from accepting Equation (32), the parallel-δB version of DCF required another important assumption. According to Equation (34), DCF study requires knowledge of the perpendicular component of the magnetic field. Therefore, an additional assumption of the equality of parallel and perpendicular fluctuations, i.e., $\delta B_\perp \approx \delta B_\parallel$, was required to make parallel-δB version of DCF applicable to magnetic field studies. Based on empirical study, this additional assumption justifying the approach was added by R. Skalidis et al. (2021). More recently, theoretical attempts were made to explain the relations that appealed to turbulence compressibility (R. Skalidis et al. 2023a). In contrast, in Section 2.2.1, we derived the relation $\delta B_\parallel \approx \delta B_\perp$ from the condition that the magnetic field is divergence-free. We did not appeal to any compressibility effects for doing this. We also successfully tested our prediction numerically for incompressible MHD turbulence.

The difficulties with understanding the physical picture behind the ST21 approach were discussed in P. S. Li et al. (2022) and in A. Lazarian et al. (2022). The latter paper, however, stated that there was "no reason to question the ST21 equation as a consequence of an empirically established fact." The fact that a similar equation was proven to hold for compressible simulations (see ST21; R. Skalidis et al. 2021) and our incompressible simulations may suggest that the effects of velocity driving are dominant.

Within this study, we do not discuss the γ-dependence of $f_2(\gamma)$. Empirically, for $\gamma = \pi/2$ Equation (37), the coefficient or $f(\pi/2) = 2/\sqrt{2}$ was proposed by ST21. Based on the analysis in A. Lazarian et al. (2022), we expect this numerical value to vary depending on the actual properties of the cascade, i.e., its composition in terms of Alfvén, slow, and fast modes.

In this paper, we get the expression given by Equation (37) based on considering a velocity-driven sub-Alfvénic turbulence. Theoretical considerations in GS95 suggested that the properties of the Alfvénic cascade are marginally affected by compressibility. For the case of trans-Alfvénic turbulence, it was numerically demonstrated that the energy exchange of Alfvén and fast/show modes is marginal (J. Cho & A. Lazarian 2003; see also J. Cho & A. Lazarian 2005). It is reasonable to expect that this is also true for sub-Alfvénic turbulence. The presence of the fast modes only marginally changes the variations of magnetic field direction (LV99). Therefore, we expect that the fluctuations in magnetic field direction are determined by Alfvénic turbulent cascade and the dependence on $\delta\phi$ that we revealed for our incompressible simulations will be valid for compressible turbulence of molecular clouds. A comparison of our incompressible results with the available compressible studies that we discuss in Section 6.3 supports this conclusion. We stress the importance of the function $f_2(\gamma)$, which we will define for different regimes elsewhere.

Since the regime of weak turbulence is not robust, it requires further studies to determine which type of turbulence driving is relevant to the astrophysical settings. For instance, the driving in R. Santos-Lima et al. (2021) induces turbulence for which the magnetic field strength should be studied using Equation (36).

Both Equations (36) and (37) assume that the dispersions of magnetic field and velocities are measured over the injection scale L. This is not always applicable. In many cases, the velocity dispersion δv is measured over the full depth of the cloud L_c, while the dispersion of magnetic field angles is measured over the available patch $L_p \times L_p$, where $L_p < L_c$. For magnetically driven turbulence, $\delta\phi$ is artificially decreased, which biases the magnetic field obtained with Equation (36) toward higher values. This effect is less pronounced for velocity-driven turbulence, as shown in Figure 6.

The difference in the variations of the positional angle with the change of the averaging block can be used to distinguish the two regimes of turbulence driving. This information is significant by itself. In terms of the DCF technique, it determines whether Equation (36) or Equation (37) should be used to obtain the magnetic field strength.

7.3. Other Approaches to DCF

7.3.1. Universal Expression for DCF: MM2 Approach

In A. Lazarian et al. (2022), modifying the DCF equations to use the velocity Alfvén Mach number M_A instead of the $\delta\phi$ was suggested. The motivation for this was that M_A could be measured not only through polarimetry but also with other techniques, e.g., using velocity gradients (A. Lazarian et al. 2018), Tsallis statistics (A. Esquivel & A. Lazarian 2010), velocity anisotropy (A. Esquivel & A. Lazarian 2011; A. Lazarian & D. Pogosyan 2012; B. Burkhart et al. 2014; D. Kandel et al. 2016) . It is important that some of the techniques measuring M_A can obtain 3D information using velocity channel maps, e.g., (A. Esquivel et al. 2015; A. Lazarian et al. 2018) or the synchrotron polarization tomography (A. Lazarian & K. H. Yuen 2018), providing better insight into media magnetization.

As shown below, this approach provides a universal form for the DCF that is valid for both velocity- and magnetic-field-driven turbulence. Equations (36) and (37) can be presented in the universal form. Indeed, for the velocity-driven case, $\delta\phi$ given by Equation (34) scales as M_A^2 according to Equation (28). Thus, instead of Equation (37) one can write

$$B_\perp \approx f(\gamma)\sqrt{4\pi\rho}\,\frac{\delta v}{M_A}. \tag{38}$$

Incidentally, the magnetically driven case, $\delta\phi \approx M_A$ and Equation (36) also transfers into Equation (38). The functions

$f(\gamma)$ may be different, and the difference should be determined by future studies.

One can take the next step and employ sonic Mach number $M_s \approx V_L/c_s$, where c_s is sound velocity instead of δv in Equation (38). This number can be measured by several techniques described in the literature (B. Burkhart et al. 2009, 2012; A. Esquivel & A. Lazarian 2010; B. Burkhart & A. Lazarian 2016).

Then, one gets the expression of the magnetic field obtained in A. Lazarian et al. (2024):

$$B_\perp \approx f_3(\gamma)\sqrt{4\pi\rho}\, c_s \frac{M_s}{M_{\rm A}}, \tag{39}$$

which universally applies, irrespective of the turbulence driving. This technique was termed MM2 in A. Lazarian et al. (2024) to reflect that it uses two Mach numbers—the Alfvén and sonic.

7.3.2. Broad View of the MM2 Approach

The advantage of this technique, termed MM2 in A. Lazarian et al. (2024) because it used two Mach numbers, is that it applies to various data sets for which $M_{\rm A}$ and M_s can be measured. This can be done by analyzing spectroscopic channel maps, where measuring the dispersion of parallel velocity is impossible. Nevertheless, both $M_{\rm A}$ and M_s can be obtained using velocity channel gradients (A. Lazarian et al. 2018; K. H. Yuen & A. Lazarian 2020). The MM2 technique has already been applied to several spectroscopic data sets, e.g., Y. Hu et al. (2021).

If the statistics of the fluctuations are related to $M_{\rm A}$ and M_s by using numerical simulations that approximate the actual astrophysical settings, then one can use the universal Equations (38) and (39) without worrying whether the turbulence is magnetically or velocity driven.

As we discussed earlier (see Figure 7), one can determine from observations whether the turbulence is velocity or magnetic field driven. Therefore, if the technique provides $M_{{\rm A},b}$, it can be transferred to $M_{\rm A}$ using Equation (28). This looks promising for obtaining magnetic field strength for various astrophysical settings. This approach deserves a dedicated study.

It is important to stress that MM2 is not just another way of rewriting the DCF formulae. It opens new horizons for new types of observational data in order to obtain magnetic field strength. For instance, the MM2 technique can also be applied to synchrotron intensity and column density maps.

Machine learning also provides a new promising way of determining $M_{\rm A}$ and M_s (see Y. Hu et al. 2024a). Machine learning can be used to determine whether turbulence is driven by magnetic or velocity fluctuations.

7.3.3. Filtering the Data Within the DCF: Comparison with DMA

Our study demonstrated that the difference in $M_{\rm A}$ and $M_{{\rm A},b}$ arises from fluid flow along the magnetic field lines. This suggests that if the velocity contributions arising from such motions are removed, then $M_{\rm A}$ and $M_{{\rm A},b}$ will coincide. This also means that one can use the traditional DCF given by Equation (36) without additional concerns about the nature of turbulence driving.

The motions along magnetic field lines for the observer are seen as motions along the mean field with the perpendicular dispersion $M_{{\rm A},b}$. By filtering out the 2D spatial frequencies $K_\parallel = 0$ and $K_\perp$ in the range of $[-M_{{\rm A},b}, M_{{\rm A},b}]$ one can remove the spatial frequencies that are affected by the fluid parallel flows. A detailed study of this approach will be done elsewhere.

Finally, we briefly compare the DCF and a more recently suggested differential measure analysis (DMA; A. Lazarian et al. 2022) approach. Within DMA, not the dispersions of magnetic field directions and linewidths but locally measured structure functions of velocity centroids and magnetic field directions are employed. The DMA approach provides many advantages, e.g., it can increase accuracy and provide detailed distributions of magnetic field. However, DMA requires more information about the turbulence properties. We treat DMA and DCF as complementary tools.

8. Discussion

8.1. Sub-Alfvénic Turbulence: Comparison with Selected Earlier Studies

8.1.1. Incompressible MHD Turbulence Studies

Our paper demonstrates that the difference in how turbulence is driven significantly changes the properties of MHD turbulence. The major finding of the present paper is the introduction of the magnetic Mach number $M_{{\rm A},b}$ that coincides with $M_{\rm A}$ for magnetically driven turbulence and is equal to $M_{\rm A}^2$ for velocity-driven turbulence. $M_{{\rm A},b}$ enters the LV99 expressions describing the properties of sub-Alfvénic MHD turbulence at small scales and the expressions that employ the LV99 formalism. These include expressions for turbulent damping of Alfvén waves, heat and matter transfer, removal of magnetic fields from star-forming clouds, superdiffusion of cosmic rays, etc.

MHD turbulence is a subject with an extended history of research (see, e.g., the book by A. Beresnyak & A. Lazarian 2019). The different regimes of MHD turbulence have been studied theoretically (e.g., S. Galtier et al. 2000; S. Nazarenko 2007; K. H. Yuen et al. 2024; S. Galtier 2023), numerically (e.g., R. Meyrand et al. 2016; R. Santos-Lima et al. 2021), and observationally (e.g., S. Zhao et al. 2024a, 2024b).

Weak Alfvénic turbulence is different from its strong counterpart that takes place at scales less than $LM_{{\rm A},b}^2$ (LV99; R. Meyrand et al. 2016). In Section 2, we stressed the importance of the perpendicular scale $LM_{{\rm A},b}$, which defines the scale at which the magnetic field fluctuations are decorrelated unless enforced by numerical schemes. Our paper demonstrates that turbulence driving profoundly affects the properties of MHD turbulence. The modification is not limited to the weak turbulence range but carries over by changing the ratio of energy in Alfvén and slow modes for the strong MHD turbulence regime (see Equation 26).

Alfvénic turbulence has been studied in many numerical papers (e.g., J. Maron & P. Goldreich 2001; L. J. Milano et al. 2001; A. Beresnyak 2012; J. Mason et al. 2012; A. Mallet et al. 2015; R. Meyrand et al. 2016). Some of them (e.g., J. Maron & P. Goldreich 2001; R. Meyrand et al. 2016) drive both velocity and magnetic field simultaneously while using Elsässer variables (W. M. Elsässer 1950) via the white noise method (e.g., L. J. Milano et al. 2001; A. Beresnyak 2012; J. Mason et al. 2012; A. Mallet et al. 2015). This driving implies that the velocity and the magnetic field are driven coherently. Since driving by velocity or magnetic field does not have any

advantages, the theoretical elegance of the Elsässer equation approach is favored for incompressible studies compared to using Equation (29). The Elsässer driving conditions ensure the equality of magnetic and kinetic energies. However, such simulations cannot answer what happens in the case of astrophysical driving that can be induced through random velocities.

Our study reveals that the isotropic velocity driving of incompressible sub-Alfvénic turbulence induces a new effect of flows along magnetic field lines. At the injection scales, these flows absorb most of the injected energy because the dynamically dominant magnetic field strongly resists the driving perpendicular to magnetic field lines. The variations of the parallel velocities V_L induce fluid pressure variations δP according to the Bernoulli equation, and this results in Equation (9), which relates the standard deviation of the parallel magnetic field fluctuation with the fluctuation in the dynamical pressure of the fluid $1/2\rho V_L^2$. Unlike the magnetic or Elsässer variable driving, for $\delta B_\parallel < B$ this induces the disparity of kinetic and magnetic energies in turbulence (see Equation (24)). The magnetic field is divergence free, which ensures the approximate equality of the magnetic fluctuations perpendicular and parallel to the mean field, i.e., $\delta B_\parallel \approx \delta B_\perp$. The dependence of sub-Alfvénic turbulence properties on the nature of turbulence driving is one of our major findings in this paper.

The closest to our approach is J. Cho et al. (2002), where the authors solve Equation (29) similarly to our current study. Their setup provides $M_A \approx 1$, meaning that the trans-Alfvénic turbulence is studied. The condition outlined in Section 2.2 converts to the perpendicular structure function for the magnetic field at large scale $SF_B \propto l_\perp^0$, while that for velocity $SF_v \propto l_\perp^1$. Figure 3 of J. Cho et al. (2002) shows a difference in structure function at the largest scale, which is consistent with our present study.

The accepted description of incompressible MHD turbulence assumes that kinetic and magnetic energies are equal for Alfvénic modes, and that the energies of Alfvén and slow modes for isotropic incompressible driving are also similar. Our study reports the violation of these two common assumptions if sub-Alfvénic turbulence is generated by isotropic velocity driving. This changes the starting point for accounting for the compressibility effects in MHD turbulence.

8.1.2. Relation to Compressible MHD Turbulence Studies

Our findings shed new light on the earlier studies of compressible MHD turbulence, which reported the dominance of kinetic over magnetic energies in J. R. Beattie et al. (2022). This and the related studies in R. Skalidis et al. (2023b) attributed this disparity to the compressibility of the MHD turbulence that they dealt with, as opposed to the classical MHD turbulence theory, e.g., GS95 theory, formulated in incompressible limit. We demonstrate that the same disparity is present in incompressible turbulence. This does not prove that the theories explaining the effect through compressibility are wrong. However, this, at least, testifies that compressibility is not the sole reason for the disparity. For us, this is suggestive that the energy disparity is a part of the fundamental properties of velocity-driven MHD turbulence that is already present in the incompressible limit. We predict that the magnetically driven compressible turbulence will not show the same significant difference between the velocity and magnetic turbulent energies.

It is well known that incompressible MHD turbulence is a reasonable approximation for realistic subsonic compressible turbulence in high-β media (see GS95). For sub-Alfvénic turbulence in high-β media, the subsonic requirement is automatically fulfilled. Therefore, the model of turbulence that we quantified applies to a wide range of astrophysical high-β plasmas, e.g., plasma in the warm and hot galactic gas, and intercluster gas. Effects of compressibility in such a nearly incompressible gas are marginal, which makes the alternative explanations based on turbulence compressibility unlikely.[16]

Potentially, the effects of compressibility may take over in low-β media. For us, it seems surprising that very different physics will provide the same result given by Equation (24). The testing with magnetic driving of turbulence in low-β media that we proposed can definitively answer whether theories that explained the disparity appealing to the effects of compressibility are correct.

At present, one may argue that Occam's razor principle suggests that there is likely to be one universal process that makes Equation (24) correct both in high and low-β media. We argued above that the compressibility explanation does not work in high-β media. An analogy in the history of turbulence research was an empirical discovery of the rapid decay of turbulence in low-β media. Initially, it was initially accepted to take place due to the coupling of Alfvénic and compressible modes. At the same time, the decay of turbulence over one eddy turnover was the theoretical prediction of incompressible MHD turbulence (GS95; LV99), which was confirmed numerically (J. Cho & E. T. Vishniac 2000). Later numerical research confirmed that in both low and high-β media the decay happens due to the fundamental nonlinearity of Alfvénic modes, which is marginally influenced by fluid compressibility (J. Cho & A. Lazarian 2002). We hope that new simulations will soon test the application of Occam's razor principle to the case at hand.

In short, in terms of the disparity of kinetic and magnetic energies in sub-Alfvénic simulations, our scope of claims is limited to the following:

1. We disprove that the presence of kinetic and magnetic energy disparity requires that the turbulence must be compressible.
2. We demonstrate that in an incompressible fluid, isotropic velocity driving of turbulence creates disparity, while magnetic driving does not induce such a disparity.
3. We suggest a hypothesis that the disparity in a compressible case can also result from the isotropic velocity driving and provide a way to test our hypothesis. We invite the community to test this hypothesis.

At the same time, we stress that the disparity between kinetic and magnetic energies given by Equation (24) in incompressible sub-Alfvénic turbulence is not the only valuable result of the paper. We also provided predictions and testing for the spectra of velocities and magnetic field, spectra slow, and Alfvén modes applicable to high-β media. Our study poses an interesting problem of testing to what extent the corresponding

[16] Indeed, appealing to velocity driving in incompressible turbulence, we get the disparity of kinetic and magnetic energies given by Equation (24). It is not conceivable that marginal compressibility in high-β media not only overrides this effect but also imposes the same relation given by Equation (24).

relations are different for low-β compressible media. This can be studied by analyzing the existing sub-Alfvénic compressible simulations.

8.1.3. Modified DCF: The Importance of the Way Turbulence is Driven

Since our study deals with incompressible turbulence, we do not discuss theories suggested to justify modifying the DCF due to effects of compressibility (see R. Skalidis et al. 2021, 2023b). Instead, we address the modifications the DCF technique required for incompressible turbulence when turbulence is velocity driven at the injection scale. The numerical evidence in the aforementioned studies testifies that our DCF modification for the case of velocity driving also approximately holds for the compressible case. While a quantitative study of compressibility's role in improving the accuracy of the DCF approach is beyond the scope of the present paper, below we provide a few considerations that may justify why compressibility effects may not significantly change the DCF approach.

From what we know about the relation of compressible and incompressible MHD (see A. Beresnyak & A. Lazarian 2019), we expect compressibility to modify the energy partition between fast mode, on the one hand, and slow and Alfvén modes, on the other. Since Alfvén modes dominate magnetic field wandering (LV99), we expect Equation (28) to hold approximately. We also expect that the flows corresponding to $k_{\parallel}=0$ will be similar in compressible and incompressible cases. In the case of velocity driving, we may expect the velocity fluctuations for $M_{\mathrm{A},b}<1$ to be dominated by flows along magnetic field lines rather than fast modes. This can explain why Equation (37) derived for the incompressible MHD turbulence in the presence of isotropic velocity driving can be valid for compressible media, which is in agreement with numerical simulations in R. Skalidis et al. (2021, 2023b). We are unaware of DCF validity studies using magnetic driving at the injection scale, so we have nothing to compare Equation (36) for the compressible case. Further studies employing the separation of modes following the procedures in J. Cho & A. Lazarian (2003) and G. Kowal & A. Lazarian (2010) will be done elsewhere to test these expectations.

8.2. Impact on Understanding of Astrophysical Processes: Selected Implications

8.2.1. Improved Analytical Description of MHD Turbulence

Below, we primarily discuss how our present results modify the conclusions reached within the earlier studies of MHD turbulence that did not consider the effects arising from velocity driving. Naturally, the list of implications is very extensive and deserves a separate study.

The transition scale from weak to strong turbulence (see Section 2) and the corresponding small-scale scaling of strong MHD turbulence are functions of $M_{\mathrm{A},b}$ (LV99). For the velocity-driven turbulence, $M_{\mathrm{A},b}$ must be related to the traditional Alfvén Mach number M_{A} via Equation (28). Thus, in the case of velocity driving of sub-Alfvénic turbulence, only a fraction of total velocity dispersion at the injection scale L can be associated with the driver of the Alfvénic cascade.

In particular, using $M_{\mathrm{A},b}$ is important for describing statistics of MHD turbulence that can be obtained from observations (A. Lazarian & D. Pogosyan 2012; D. Kandel et al. 2016, 2017a, 2017b) and applying the corresponding tools to explaining the observations. In particular, D. Kandel et al. (2018) found that the Plank result of B/E power ratio is consistent with interstellar media being sub-Alfvénic. If turbulence in ISM is velocity driven, then the Alfvén Mach number in D. Kandel et al. (2018) should be identified with $M_{\mathrm{A},b}$. The upper limit that was found in D. Kandel et al. (2018), namely, $M_{\mathrm{A},b}<0.5$ satisfies the observational data. This limit translates, according to Equation (28), into $M_{\mathrm{A}}<0.7$, which is less restrictive in terms of media magnetization.

8.2.2. Diffusion and Acceleration of Cosmic Rays

The analytical theory of MHD turbulence is critical for describing the propagation and acceleration of cosmic rays (CRs; see R. Schlickeiser 2002). Sub-Alfvénic turbulence is typical for the diffuse ISM and galactic halo, where CRs propagate (V. L. Ginzburg & S. I. Syrovatskii 1964). In addition, turbulence can be important for the stochastic acceleration of energetic particles (see V. S. Ptuskin 1988; P. Blasi 2000; G. Brunetti & A. Lazarian 2007a).

The most trivial consequence of our paper is that in the study of CRs, $M_{\mathrm{A},b}$ should be employed. This requires distinguishing the cases of velocity- and magnetic-field-driven turbulence.

The amplitude and anisotropy of the magnetic fluctuations critically affect both the CRs' acceleration and propagation through resonant scattering (see B. D. G. Chandran 2000; H. Yan & A. Lazarian 2002, 2003; S. Xu & H. Yan 2013; Y. Hu et al. 2022c; S. Maiti et al. 2022). Our results show that for turbulence's isotropic velocity driving, the magnetic fluctuations' spectrum scales as k^{-1} for scales from LM_{A} to L. This has significant consequences for the magnetic field wandering that determines perpendicular to mean magnetic field superdiffusion of CRs (A. Lazarian & H. Yan 2014).

It is also significant that Alfvénic turbulence is an important factor in suppressing the streaming instability that regulates the transport of CRs (H. Yan & A. Lazarian 2002; A. J. Farmer & P. Goldreich 2004; A. Lazarian et al. 2016). Incidentally, this effect is also essential for driving galactic winds (see A. Lazarian & S. Xu 2022). Less energy in magnetic turbulence decreases the suppression efficiency.

Another funding in this paper is that the slow mode magnetic fluctuations do not change their amplitude in the $[LM_{\mathrm{A},b}, L]$ range for the velocity driving in high β medium. These fluctuations dominate the effect of magnetic mirror diffusion (S. Xu & A. Lazarian 2020; A. Lazarian & S. Xu 2021) and acceleration (A. Lazarian & S. Xu 2023). Our present study predicts an increase of the efficiency of these processes.

Transient time damping (TTD) acceleration has a vital effect on CR propagation and acceleration (see B. R. Ragot & R. Schlickeiser 1998; G. Brunetti & A. Lazarian 2007b; F. Holguin et al. 2019). Magnetic compressions associated with slow modes can dominate the process (see S. Xu & A. Lazarian 2018). Our study shows that the amplitude of such compressions may be $\sim M_{\mathrm{A}}^{-1}$ larger than the Alfvén ones (see Figure 8). This factor should increase the importance of slow modes in TTD acceleration for high-β medium.

We do not dwell upon the quantitative consequences of these effects. The improved understanding of sub-Alfvénic turbulence attained in the present study deeply impacts CR physics. The quantitative discussion of CRs' propagation and acceleration will be provided elsewhere.

8.2.3. Evolution of Interstellar Medium and Star Formation

Magnetized turbulence is critical in star formation (C. F. McKee & E. C. Ostriker 2007). Thus, accounting for the disparity of kinetic and magnetic turbulent energies is vital for understanding star formation processes. More energy associated with fluid motions along magnetic field lines tends to produce a more prominent turbulent concentration of matter. This is important for the formation and evolution of molecular clouds. In particular, this can contribute to forming density structures perpendicular to the magnetic field (S. Xu et al. 2019b; J. R. Beattie & C. Federrath 2020).

At the same time, according to the model of the formation of filaments parallel to the magnetic field (see S. Xu et al. 2019a), more energy in slow modes reported in our study results in a higher contrast of such filaments. For instance, this can provide the compression necessary to explain the higher rate of CO formation within the striation observed in the Polaris Flare (R. Skalidis et al. 2023a).

The relative increase of the slow mode amplitude can be one of the causes of the appearance of the small ionized and neutral structures observed in the interstellar medium and discussed in C. Heiles (1997). The alternative suggestions attempting to explain these mysterious structures include the current sheets in fully ionized plasmas (P. Goldreich & S. Sridhar 2006) and a viscosity-damped regime of MHD turbulence in partially ionized gas (J. Cho et al. 2003; A. Lazarian 2007). Both suggestions have shortcomings; thus, accounting for enhancing the relative amplitude of pseudo-Alfvén/slow modes that we reported in the paper is important. One can argue that the corresponding magnetic fluctuations cause the enhancements of ionized gas, which can alleviate solving the SINs puzzle. However, to what extent this can be true requires more studies of compressible MHD turbulence in partially ionized gas (see Y. Hu et al. 2024b).

The process of magnetic field diffusion induced by turbulent reconnection, i.e., the reconnection diffusion (A. Lazarian 2005, 2006; R. Santos-Lima et al. 2010; A. Lazarian 2014), is an essential process for the removal of magnetic fields from molecular clouds. The predictions for the rate of the reconnection diffusion in sub-Alfvénic case were confirmed in R. Santos-Lima et al. (2021) for the case that corresponds to $E_k = E_B$ (see Section 5.1). For velocity driving of turbulence, the analytical dependences for the reconnection diffusion rate on M_A should be reconsidered.

We note that numerous earlier numerical studies dealing with interstellar turbulence (C. Federrath et al. 2008; E. Vázquez-Semadeni et al. 2010; J. Ballesteros-Paredes et al. 2011; J. R. Beattie et al. 2022) reported the importance of the driving of fluid motions along the magnetic field. Our present study relates these flows with the velocity driving of turbulence and quantifies the resulting statistics.

8.3. Drivers of Galactic Turbulence

The nature of galactic turbulence is a hotly debated subject. Stellar winds, supernovae explosions, and magneto-rotational instability are examples of turbulent drivers proposed in the literature (see C. F. McKee & E. C. Ostriker 2007). On the contrary, some authors advocate turbulence generation through gravitational instability (see E. Vázquez-Semadeni et al. 2017). Our study demonstrates the significant role that driving can have on the properties of turbulence.

Observational studies of galactic turbulence (J. W. Armstrong et al. 1995; A. Chepurnov & A. Lazarian 2010; S. Xu & B. Zhang 2016; K. H. Yuen et al. 2022) suggest the existence of a universal cascade that starts at a scale comparable with the galactic scale height and proceeds to the dissipation scale over many orders of scales. This is consistent with driving on scales significantly exceeding the scale of molecular clouds. Turbulence driving at the scale height of the galactic disk provides a possible explanation of the observed turbulence properties. Expanding supernovae superbubbles can be a possible driver along with gravitational perturbations responsible for the emergence of the Radcliff wave (J. Alves et al. 2020).

We expect that most of the instabilities are induced by either stellar evolution feedback or gravitational instabilities to induce turbulence through velocity driving. The consequences that follow from our study arise when the turbulence is driven isotropically by sub-Alfvénic driving. It is unclear to what extent this applies to our galaxy or other spiral galaxies.

Within the picture of the global turbulence cascade, it is not reliable to evaluate the nature of turbulence driving by detecting sub-Alfvénic turbulence over a small patch of the sky. The observed anisotropy of turbulence may result from the measurements over scales significantly smaller than the driving scale. At the same time, as discussed in this paper, the measurements of magnetic fluctuations across scales and their comparison with velocity fluctuations can answer the question of whether the sub-Alfvénic turbulence was velocity driven. Thus, the peculiar features of sub-Alfvénic turbulence that we revealed in the present study should be relevant in the galactic context.

Like most papers dealing with MHD turbulence, our paper assumes an isotropic turbulence driving. This assumption is not guaranteed to be true in realistic astrophysical settings. Moreover, even if the injection scale of the isotropic driving is $\sim$100 pc, the universal turbulent cascade can excite motions at the scale of individual molecular clouds (see K. H. Yuen et al. 2022). Within this study, we do not address how turbulence anisotropy changes in multiphase media (see K. W. Ho et al. 2023). This and other questions will be addressed in subsequent studies.

9. Summary

We explored how fundamental properties of incompressible MHD turbulence changed by the way of driving turbulence. We identified a new effect: the properties of turbulence radically change depending on whether it is driven through velocity or magnetic fluctuations. Our findings can be briefly summarized as follows:

1. The disparity of the energies of magnetic and velocity turbulence arises from the velocity driving of turbulence. The magnetic driving of turbulence provides similar amounts of energy in kinetic and magnetic fluctuations.
2. For velocity driving, fluid streams along stochastic magnetic field lines, and the kinetic energy of such a flow exceeds the energy of turbulent magnetic field fluctuations by a factor $\sim M_A^{-2}$. Our comparison with earlier compressible MHD studies suggests that this effect arises from how turbulence is driven rather than fluid compressibility. We suggested a way of testing this hypothesis.

3. For velocity driving of turbulence, fluid flow imprints the magnetic field stochasticity, resulting in the kinetic energy spectrum E_K scaling $\sim k^{-2}$. The magnetic fluctuations slowly evolve near the injection scale, corresponding to the $E_b \sim k^{-1}$ cascade.
4. Velocity-driven turbulence transfers more energy to slow modes than Alfvénic modes, which induces numerous astrophysical implications.

The velocities and magnetic field spectra coincide if the turbulence is magnetically driven at the injection scale.

In terms of astrophysical implications, our study demonstrates the following:

1. The importance of accounting for the nature of turbulence driving for evaluating the effects of turbulence on key astrophysical processes, e.g., on star formation, formation of filaments, cosmic ray propagation, and acceleration.
2. The traditional DCF approach for obtaining the magnetic field strength from observations must be modified depending on the turbulence driving.
3. We outline a possible way to determine the nature of turbulent driving from observations and show that measuring sonic and Alfvén Mach numbers allows us to obtain the magnetic field using a universal expression that does not depend on the nature of turbulent driving.

Our numerical testing is limited by incompressible MHD simulations. Some of the relations derived in this paper correspond to those obtained earlier empirically and were attributed to the effects of compressibility. We hypothesize these effects can also arise due to velocity driving employed in the earlier studies. We predict that in the case of magnetic driving, the differences between kinetic and magnetic energies will be significantly reduced in the case of compressible simulations. This calls for more studies exploring the extent that the fundamental properties of sub-Alfvénic MHD turbulence we explored in the incompressible regime carry over to the case when the compressibility is very important, i.e., for the case of turbulence in low-β plasmas.

Acknowledgments

We thank Chris McKee for reading this paper and providing valuable suggestions on our presentation and discussions of the role of the slow modes in MHD turbulence. We thank Andrey Beresnyak for discussing the effects of boundary conditions on the simulation results, Reinaldo Santos-Lima for discussing weak turbulence simulations, and Dmitri Pogosyan for discussing the relation of parallel and perpendicular fluctuations. We also thank Jungyeon Cho and Hui Li for discussing v_A variation and the nature of $k_\parallel = 0$ modes in MHD turbulence. A.L. and K.W.H. acknowledge the support of NASA ATP AAH7546 and NSF 2307840. K.H.Y. thanks James Beattie for discussing the role of $k_\parallel = 0$ modes. The research presented in this article was supported by the LDRD program of LANL with project Nos. 20220107DR (K.W.H.) and 20220700PRD1 (K.H.Y.), and a US DOE Fusion Energy Science project. This research used resources from the LANL Institutional Computing Program (y23_filaments), supported by the DOE NNSA Contract No. 89233218CNA000001. E.V. acknowledges the support from the AAS. This research also used resources of NERSC with award numbers FES-ERCAP-m4239 (PI: K.H.Y.) and m4364 (PI: K.W.H.). We acknowledge Michael Halfmoon for additional NERSC time needed for this project. We also acknowledge the hospitality of KITP and its associated grant No. NSF PHY-1748958.

Data Availability

The data underlying this article will be shared on reasonable request to the corresponding author.

Software: MHDFlows (K. W. Ho 2022), FourierFlows (N. C. Constantinou et al. 2023).

Appendix
Properties of Slow and Fast Modes

In Section 2.2.1, we discussed how fluctuations of velocities along magnetic field lines produce fluctuations in parallel magnetic field strength for incompressible turbulence, i.e., turbulence in the media corresponding to $\beta \to \infty$. However, the effect is generic for media with arbitrary β.

Figure 10 illustrates the effect. The mean magnetic field is in the vertical direction and the fluid is pumped along the magnetic field. If the fluid flows along the magnetic field with mean velocity V, the variations of flow velocity δV result in the variations of fluid pressure that are compensated by the compressions/expansions of the magnetic flux tube. The corresponding variations of the flux tube thickness can be presented as a superposition of magnetosonic waves.

Having a magnetic flux tube with thickness modulated by the flow, one can consider how slow and fast modes can be produced through such a modulation. Consider first a slow waves effect. Their wavevector $\boldsymbol{k}$ is perpendicular to the wave front $\hat{\theta}$ and the vector of slow mode transposition $\boldsymbol{\zeta}_s$ is between $\hat{\theta}$ and $\boldsymbol{B}_0$. The angle between $\hat{\theta}$ and $\boldsymbol{\zeta}_s$ depends on plasma β, the two vectors get parallel for $\beta \to \infty$ and get perpendicular for $\beta \to 0$. In the former case, slow modes are degenerate with Alfvén waves because they do not induce any compression of either fluid or magnetic field. The variations of the magnetic flux tube thickness shown in Figure 10 can be achieved by slow modes of different wavelengths and different directions of $\boldsymbol{k}$. This implies that the modulation of the flux tube thickness induced by the fluid (see Figure 10) can generate a spectrum of slow waves with different $\boldsymbol{k}$. In particular, for the incompressible case, the excited slow modes with $\boldsymbol{k}$ perpendicular to $\boldsymbol{B}_0$ and correspond to the "condensate" with $k_\parallel = 0$ that we study in our next paper. The exact composition and the properties of the magnetosonic waves that the Bernoulli effect can generate is beyond the scope of the present paper.

The fast modes have their transposition vector $\boldsymbol{\zeta}_f$ between the direction $\boldsymbol{k}$ and the direction perpendicular to $\boldsymbol{B}_0$, i.e., the $\boldsymbol{k}_\perp$ direction. The relative orientation of $\boldsymbol{k}$ depends on plasma β. $\boldsymbol{\zeta}_f$ is aligned with $\boldsymbol{k}$ in incompressible fluids and gets perpendicular to $\boldsymbol{k}$ when $\beta \to 0$. Fast modes do not exist for the incompressible fluid because their speed is infinite. Thus, our paper does not consider the effect of fast waves. However, magnetosonic perturbations corresponding to fast modes become more important as β decreases. For $\beta \to 0$, fast waves responsible for the modulation of magnetic flux as shown in Figure 10 are moving parallel to $\boldsymbol{B}_0$.

For a finite β, the fluctuation $\delta B_\parallel$ defined by Equation (9) is achieved by combining slow and fast modes with the composition of modes being a function of β. The contribution of fast modes is marginal for high β, but it gets dominant for $\beta \to 0$. In the latter case, slow modes correspond to sound waves propagating along magnetic field. Such waves cannot originate from the magnetic field compressions arising from the Bernoulli effect.

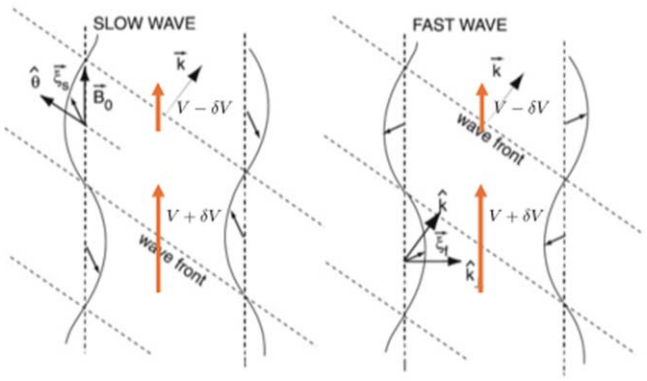

Figure 10. Red vectors correspond to the velocities of the flow along the flux tube. Slow and fast waves in real space ($\boldsymbol{B}_0$–$\boldsymbol{k}$ plane). The directions of displacement vectors for a slow wave (left-hand panel) and a fast wave (right-hand panel) are shown. Note that the transposition vector for the slow mode $\hat{\xi}_s$ lies between the wave front $\hat{\theta}$ direction and $\boldsymbol{B}_0$ ($=\boldsymbol{k}_\parallel$) and $\hat{\xi}_f$ between $\boldsymbol{k}$ and $\boldsymbol{k}_\perp$. Note that $\hat{\theta}$ is perpendicular to $\boldsymbol{k}$ and parallel to the wave front (modified from CLV03).

ORCID iDs

A. Lazarian https://orcid.org/0000-0002-7336-6674
Ka Wai Ho https://orcid.org/0000-0003-3328-6300
Ka Ho Yuen https://orcid.org/0000-0003-1683-9153
Ethan Vishniac https://orcid.org/0000-0002-2307-3857

References

Alvelius, K. 1999, PhFl, 11, 1880
Alves, J., Zucker, C., Goodman, A. A., et al. 2020, Natur, 578, 237
Andersson, B. G., Lazarian, A., & Vaillancourt, J. E. 2015, ARA&A, 53, 501
Armstrong, J. W., Rickett, B. J., & Spangler, S. R. 1995, ApJ, 443, 209
Bai, X.-N. 2022, ApJ, 928, 112
Ballesteros-Paredes, J., Hartmann, L. W., Vázquez-Semadeni, E., Heitsch, F., & Zamora-Avilés, M. A. 2011, MNRAS, 411, 65
Banerjee, S., & Galtier, S. 2013, PhRvE, 87, 013019
Batchelor, G. K. 2000, An Introduction to Fluid Dynamics (Cambridge: Cambridge Univ. Press)
Beattie, J. R., & Federrath, C. 2020, MNRAS, 492, 668
Beattie, J. R., Federrath, C., & Seta, A. 2020, MNRAS, 498, 1593
Beattie, J. R., Krumholz, M. R., Skalidis, R., et al. 2022, MNRAS, 515, 5267
Beresnyak, A. 2012, MNRAS, 422, 3495
Beresnyak, A. 2014, ApJL, 784, L20
Beresnyak, A., & Lazarian, A. 2006, ApJL, 640, L175
Beresnyak, A., & Lazarian, A. 2009, ApJ, 702, 1190
Beresnyak, A., & Lazarian, A. 2019, Turbulence in Magnetohydrodynamics (Boston, MA: De Gruyter)
Blasi, P. 2000, ApJL, 532, L9
Boldyrev, S. 2006, PhRvL, 96, 115002
Boldyrev, S., Perez, J. C., Mason, J., & Cattaneo, F. 2007, APS Meeting Abstracts, 49, PO7.001
Brunetti, G., & Lazarian, A. 2007a, MNRAS, 378, 245
Brunetti, G., & Lazarian, A. 2007b, HiA, 14, 97
Burkhart, B., Falceta-Gonçalves, D., Kowal, G., & Lazarian, A. 2009, ApJ, 693, 250
Burkhart, B., & Lazarian, A. 2016, ApJ, 827, 26
Burkhart, B., Lazarian, A., Balsara, D., Meyer, C., & Cho, J. 2015, ApJ, 805, 118
Burkhart, B., Lazarian, A., & Gaensler, B. M. 2012, ApJ, 749, 145
Burkhart, B., Lazarian, A., Leão, I. C., de Medeiros, J. R., & Esquivel, A. 2014, ApJ, 790, 130
Chandran, B. D. G. 2000, ApJ, 529, 513
Chandrasekhar, S., & Fermi, E. 1953, ApJ, 118, 113
Chepurnov, A., & Lazarian, A. 2010, ApJ, 710, 853
Cho, J., & Lazarian, A. 2002, PhRvL, 88, 245001
Cho, J., & Lazarian, A. 2003, MNRAS, 345, 325
Cho, J., & Lazarian, A. 2005, ThCFD, 19, 127
Cho, J., Lazarian, A., & Vishniac, E. T. 2002, ApJ, 564, 291
Cho, J., Lazarian, A., & Vishniac, E. T. 2003, ApJ, 595, 812
Cho, J., & Vishniac, E. T. 2000, ApJ, 539, 273
Constantinou, N. C., Wagner, G. L., Palóczy, A., et al. 2023, FourierFlows/FourierFlows.jl: v0.10.3, Zenodo, doi:10.5281/zenodo.7631539
Crutcher, R. M., Wandelt, B., Heiles, C., Falgarone, E., & Troland, T. H. 2010, ApJ, 725, 466
Davidson, P. A. 2004, Turbulence: An Introduction for Scientists and Engineers (Oxford: Oxford Univ. Press)
Davis, L. 1951, PhRv, 81, 890
Elsässer, W. M. 1950, PhRv, 79, 183
Esquivel, A., & Lazarian, A. 2010, ApJ, 710, 125
Esquivel, A., & Lazarian, A. 2011, ApJ, 740, 117
Esquivel, A., Lazarian, A., & Pogosyan, D. 2015, ApJ, 814, 77
Eyink, G., Vishniac, E., Lalescu, C., et al. 2013, Natur, 497, 466
Eyink, G. L., Lazarian, A., & Vishniac, E. T. 2011, ApJ, 743, 51
Farmer, A. J., & Goldreich, P. 2004, ApJ, 604, 671
Federrath, C., Klessen, R. S., Iapichino, L., & Beattie, J. R. 2021, NatAs, 5, 365
Federrath, C., Klessen, R. S., & Schmidt, W. 2008, ApJL, 688, L79
Federrath, C., Rathborne, J. M., Longmore, S. N., et al. 2016, ApJ, 832, 143
Galtier, S. 2023, JPlPh, 89, 905890205
Galtier, S., Nazarenko, S. V., Newell, A. C., & Pouquet, A. 2000, JPlPh, 63, 447
Ginzburg, V. L., & Syrovatskii, S. I. 1964, The Origin of Cosmic Rays (Oxford: Pergamon)
Goldreich, P., & Sridhar, S. 1995, ApJ, 438, 763
Goldreich, P., & Sridhar, S. 2006, ApJL, 640, L159
Heiles, C. 1997, ApJ, 481, 193
Higdon, J. C. 1984, ApJ, 285, 109
Ho, K. W. 2022, MHDFlows.jl, v.0.2.1b, Zenodo, doi:10.5281/zenodo.8242702
Ho, K. W., & Lazarian, A. 2021, ApJ, 911, 53
Ho, K. W., & Lazarian, A. 2023, MNRAS, 520, 3857
Ho, K. W., Yuen, K. H., Flauger, R., & Kritsuk, A. G. 2024a, arXiv:2410.13244
Ho, K. W., Yuen, K. H., & Lazarian, A. 2023, MNRAS, 521, 230
Ho, K. W., Yuen, K. H., & Lazarian, A. 2024b, arXiv:2407.14199
Holguin, F., Ruszkowski, M., Lazarian, A., Farber, R., & Yang, H.-Y. K. 2019, MNRAS, 490, 1271
Hopkins, P. F., Squire, J., Chan, T. K., et al. 2021, MNRAS, 501, 4184
Hu, Y., Lazarian, A., & Stanimirović, S. 2021, ApJ, 912, 2
Hu, Y., Lazarian, A., Wu, Y., & Fu, C. 2024a, MNRAS, 527, 11240
Hu, Y., Lazarian, A., & Xu, S. 2022a, MNRAS, 512, 2111
Hu, Y., Xu, S., Arzamasskiy, L., Stone, J. M., & Lazarian, A. 2024b, MNRAS, 527, 3945
Hu, Y., Xu, S., Stone, J. M., & Lazarian, A. 2022c, ApJ, 941, 133
Iroshnikov, P. S. 1964, SvA, 7, 566
Kandel, D., Lazarian, A., & Pogosyan, D. 2016, MNRAS, 461, 1227
Kandel, D., Lazarian, A., & Pogosyan, D. 2017a, MNRAS, 464, 3617
Kandel, D., Lazarian, A., & Pogosyan, D. 2017b, MNRAS, 470, 3103
Kandel, D., Lazarian, A., & Pogosyan, D. 2018, MNRAS, 478, 530
Kolmogorov, A. 1941, DoSSR, 30, 301
Kowal, G., Falceta-Gonçalves, D. A., Lazarian, A., & Vishniac, E. T. 2017, ApJ, 838, 91
Kowal, G., & Lazarian, A. 2010, ApJ, 720, 742
Kraichnan, R. H. 1965, PhFl, 8, 1385
Krumholz, M. R., Crocker, R. M., Xu, S., et al. 2020, MNRAS, 493, 2817
Lazarian, A. 2005, in AIP Conf. Ser. 784, Magnetic Fields in the Universe: From Laboratory and Stars to Primordial Structures, ed. E. M. de Gouveia dal Pino, G. Lugones, & A. Lazarian (Melville, NY: AIP), 42
Lazarian, A. 2006, ApJL, 645, L25
Lazarian, A. 2007, in ASP Conf. Ser. 365, SINS—Small Ionized and Neutral Structures in the Diffuse Interstellar Medium, ed. M. Haverkorn & W. M. Goss (San Francisco, CA: ASP), 324
Lazarian, A. 2014, SSRv, 181, 1
Lazarian, A. 2016, ApJ, 833, 131
Lazarian, A., Eyink, G. L., Jafari, A., et al. 2020, PhPl, 27, 012305
Lazarian, A., Kowal, G., Takamoto, M., de Gouveia Dal Pino, E. M., & Cho, J. 2016, in Magnetic Reconnection (Astrophysics and Space Science Library) Vol. 427 ed. W. Gonzalez & E. Parker (Cham: Springer), 409
Lazarian, A., & Pogosyan, D. 2012, ApJ, 747, 5
Lazarian, A., Santos-Lima, R., & de Gouveia Dal Pino, E. 2010, ASP Conf. Ser. 429, Numerical Modeling of Space Plasma Flows, ed. N. V. Pogorelov, E. Audit, & G. P. Zank (San Francisco, CA: ASP), 113

Lazarian, A., & Vishniac, E. T. 1999, ApJ, 517, 700
Lazarian, A., & Xu, S. 2021, ApJ, 923, 53
Lazarian, A., & Xu, S. 2022, FrP, 10, 702799
Lazarian, A., & Xu, S. 2023, ApJ, 956, 63
Lazarian, A., Xu, S., & Hu, Y. 2023, FrASS, 10, 1154760
Lazarian, A., & Yan, H. 2014, ApJ, 784, 38
Lazarian, A., & Yuen, K. H. 2018, ApJ, 865, 59
Lazarian, A., Yuen, K. H., Ho, K. W., et al. 2018, ApJ, 865, 46
Lazarian, A., Yuen, K. H., & Pogosyan, D. 2022, ApJ, 935, 77
Lazarian, A., Yuen, K. H., & Pogosyan, D. 2024, ApJ, 974, 237
Li, P. S., Lopez-Rodriguez, E., Ajeddig, H., et al. 2022, MNRAS, 510, 6085
Lithwick, Y., & Goldreich, P. 2001, ApJ, 562, 279
Liu, J., Zhang, Q., & Qiu, K. 2022, FrASS, 9, 943556
Maiti, S., Makwana, K., Zhang, H., & Yan, H. 2022, ApJ, 926, 94
Makwana, K. D., & Yan, H. 2020, PhRvX, 10, 031021
Malik, S., Yuen, K. H., & Yan, H. 2023, MNRAS, 524, 6102
Malik, S., Yuen, K. H., & Yan, H. 2024, ApJ, 965, 65
Mallet, A., Schekochihin, A. A., & Chandran, B. D. G. 2015, MNRAS, 449, L77
Maron, J., & Goldreich, P. 2001, ApJ, 554, 1175
Mason, J., Perez, J. C., Boldyrev, S., & Cattaneo, F. 2012, PhPl, 19, 055902
McKee, C. F., & Ostriker, E. C. 2007, ARA&A, 45, 565
Meyrand, R., Galtier, S., & Kiyani, K. H. 2016, PhRvL, 116, 105002
Milano, L. J., Matthaeus, W. H., Dmitruk, P., & Montgomery, D. C. 2001, PhPl, 8, 2673
Nazarenko, S. 2007, NJPh, 9, 307
Nazarenko, S. 2011, Wave Turbulence (Lecture Notes in Physics) Vol. 825 (Berlin: Springer)
Ng, C. S., & Bhattacharjee, A. 1996, ApJ, 465, 845
Orszag, S. A. 1971, JAtS, 28, 1074
Ostriker, E. C. 2003, in Turbulence and Magnetic Fields in Astrophysics (Lecture Notes in Physics) Vol. 614 ed. E. Falgarone & T. Passot (Berlin: Springer), 252
Pavaskar, P., Yuen, K. H., Yan, H., & Malik, S. 2024, arXiv:2405.17985
Petrosian, V., Yan, H., & Lazarian, A. 2006, ApJ, 644, 603
Ptuskin, V. S. 1988, SvAL, 14, 255
Ragot, B. R., & Schlickeiser, R. 1998, APh, 9, 79
Richardson, L. F. 1922, Weather Prediction by Numerical Process (Cambridge: Cambridge Univ. Press)
Santos-Lima, R., Guerrero, G., de Gouveia Dal Pino, E. M., & Lazarian, A. 2021, MNRAS, 503, 1290
Santos-Lima, R., Lazarian, A., de Gouveia Dal Pino, E. M., & Cho, J. 2010, ApJ, 714, 442
Schekochihin, A. A., Nazarenko, S. V., & Yousef, T. A. 2012, PhRvE, 85, 036406
Schlickeiser, R. 2002, in Cosmic Ray Astrophysics, ed. R. Schlickeiser (Berlin: Springer)
Skalidis, R., Gkimisi, K., Tassis, K., et al. 2023a, A&A, 673, A76
Skalidis, R., Sternberg, J., Beattie, J. R., Pavlidou, V., & Tassis, K. 2021, A&A, 656, A118
Skalidis, R., & Tassis, K. 2021, A&A, 647, A186
Skalidis, R., Tassis, K., & Pavlidou, V. 2023b, A&A, 672, L3
Stone, J. M., Ostriker, E. C., & Gammie, C. F. 1998, ApJL, 508, L99
Vázquez-Semadeni, E., Colín, P., Gómez, G. C., Ballesteros-Paredes, J., & Watson, A. W. 2010, ApJ, 715, 1302
Vázquez-Semadeni, E., González-Samaniego, A., & Colín, P. 2017, MNRAS, 467, 1313
Xu, S., Garain, S. K., Balsara, D. S., & Lazarian, A. 2019a, ApJ, 872, 62
Xu, S., Ji, S., & Lazarian, A. 2019b, ApJ, 878, 157
Xu, S., & Lazarian, A. 2016, ApJ, 833, 215
Xu, S., & Lazarian, A. 2018, ApJ, 868, 36
Xu, S., & Lazarian, A. 2020, ApJ, 894, 63
Xu, S., & Lazarian, A. 2022, ApJ, 925, 48
Xu, S., & Yan, H. 2013, ApJ, 779, 140
Xu, S., & Zhang, B. 2016, ApJ, 824, 113
Yan, H., & Lazarian, A. 2002, PhRvL, 89, B1102+
Yan, H., & Lazarian, A. 2003, ApJL, 592, L33
Yan, H., & Lazarian, A. 2008, ApJ, 673, 942
Yang, L., Li, H., Guo, F., et al. 2020, ApJL, 901, L22
Yang, L. P., Li, H., Li, S. T., et al. 2019, MNRAS, 488, 859
Yuen, K. H., Ho, K. W., Law, C. Y., Chen, A., & Lazarian, A. 2022, arXiv:2204.13760
Yuen, K. H., Ho, K. W., Law, C. Y., & Chen, A. 2024, RvMPP, 8, 21
Yuen, K. H., & Lazarian, A. 2020, ApJ, 898, 65
Yuen, K. H., Li, H., & Yan, H. 2024, RvMPP, 8, 21
Yuen, K. H., Yan, H., & Lazarian, A. 2023, MNRAS, 521, 530
Zhao, S., Yan, H., Liu, T. Z., Yuen, K. H., & Shi, M. 2024a, ApJ, 962, 89
Zhao, S., Yan, H., Liu, T. Z., Yuen, K. H., & Wang, H. 2024b, NatAs, 8, 725